ISSN 1980-9743

Soils and Rocks

An International Journal of Geotechnical and Geoenvironmental Engineering

Volume 32, N. 3
September-December 2009

Soils and Rocks
Volume 32, N.3
2009

Soils and Rocks is an International Journal of Geotechnical and Geoenvironmental Engineering published by

ABMS - Brazilian Association for Soil Mechanics and Geotechnical Engineering
Av. Prof. Almeida Prado, 532, IPT/DEC-Prédio 54
05508-901 São Paulo, SP
Brazil

ABGE - Brazilian Association for Engineering Geology and the Environment
Av. Prof. Almeida Prado, 532, IPT/DIGEO- Prédio 59
05508-901 São Paulo, SP
Brazil

SPG – Portuguese Geotechnical Society
LNEC, Avenida do Brasil, 101
1700-066 Lisboa
Portugal

Issue Date: *December 2009*

Issue: *3,200 copies*

Manuscript Submission: *For review criteria and manuscript submission information, see Instructions for Authors at the end.*

SOILS and ROCKS

An International Journal of Geotechnical and Geoenvironmental Engineering

Editor Ennio Marques Palmeira - University of Brasília, Brazil

Co-editor Ricardo Oliveira - COBA, Portugal

Soils and Rocks publishes papers in English in the broad fields of Geotechnical Engineering, Engineering Geology and Geoenvironmental Engineering. The Journal is published in April, August and December. Subscription price is US$ 90.00 per year. The journal, with the name "Solos e Rochas", was first published in 1978 by the Graduate School of Engineering-Federal University of Rio de Janeiro (COPPE-UFRJ). In 1980 it became the official magazine of the Brazilian Association for Soil Mechanics and Geotechnical Engineering (ABMS), acquiring the national character that had been the intention of its founders. In 1986 it also became the official Journal of the Brazilian Association for Engineering Geology and the Environment (ABGE) and in 1999 became the Latin American Geotechnical Journal, following the support of Latin-American representatives gathered for the Pan-American Conference of Guadalajara (1996). In 2007 the journal acquired the status of an international journal under the name of Soils and Rocks, published by the Brazilian Association for Soil Mechanics and Geotechnical Engineering (ABMS), Brazilian Association for Engineering Geology and the Environment (ABGE) and Portuguese Geotechnical Society (SPG).

Soils and Rocks

1978,	1 (1, 2)
1979,	1 (3), 2 (1,2)
1980-1983,	3-6 (1, 2, 3)
1984,	7 (single number)
1985-1987,	8-10 (1, 2, 3)
1988-1990,	11-13 (single number)
1991-1992,	14-15 (1, 2)
1993,	16 (1, 2, 3, 4)
1994-2007,	17-31 (1, 2, 3)
2009,	**32 (1, 2, 3)**

ISSN 1980-9743 CDU 624.131.1

ISSN 1980-9743

SOILS and ROCKS

An International Journal of Geotechnical and Geoenvironmental Engineering

Publication of

ABMS - Brazilian Association for Soil Mechanics and Geotechnical Engineering
ABGE - Brazilian Association for Engineering Geology and the Environment
SPG - Portuguese Geotechnical Society

Volume 32, N. 3, September-December 2009

Table of Contents

Articles

Soils and Rocks
v. 32, n. 3

An Experimental Study on Scale Effects in Rock Mass Joint Strength

Manuel J.A. Leal Gomes, Carlos Dinis da Gama

Abstract. A series of laboratory tests were conducted on matched rock joint samples, no larger than 16 x 16 cm^2 of section, which were extracted from an artificial joint, having 4.32 m^2 in area, carved in a porphyritic granite block. These tests (1200 pull tests and 200 trials conducted in a sliding machine) involved the systematic levelling of sample middle planes and lead to conclusions that are discrepant with respect to conventional ideas admitted about rock-mass joint mechanics. Those discrepancies are: a) Larger matched samples showed higher strengths in the dilating phase of the sliding tests rather than those from small matched samples; b) Sample shear strengths probably depend on the transverse widths, when *JRC*, *JCS* and σ_n (the average normal stress on the rock mass joint) are high, thus inhibiting the use of stability analysis by common slope stability methods such as Fellenius'; c) At the dilating sliding phases, the mechanics of matched joints is essentially different from that of mismatched joints, as the former brings about inverse scale effects (represented by positive exponential regressions) and the latter involves normal scale effects (represented by negative exponential regressions). The results obtained upon those lab tests do not agree with those reported from *in situ* experiments, as well as the actual behaviour of natural joints. The obtained moderate correlation coefficients do not allow the consideration of these findings as physical laws, nevertheless they do represent certain types of rock mass joint behaviour, or simply useful generic rules. Thus, the subject is full of surprises, as the authors show in text.

Keywords: rock joints, scale effects, dilating sliding phase, matched and mismatched joints, pull-tests, joint strength models, experimental *JRC*.

1. Introduction

Several authors (Charrua Graça, 1985; Cunha, 1990; Bandis, 1990) who contributed to the current state of the art on scale effects in rock joint strength, noted a rather strange progression. Before the Seventies, most authors studying the problem - sometimes using rock joint samples with large areas - found inverse scale effects (that is, increasing average strength values as sample dimensions increase, tending towards an asymptotic value (as explained by the so called representative elementary volume, REV). This behaviour is represented by positive exponential regressions. Probably influenced by the classic experimental works by Barton & Choubey, 1977 and Bandis, 1980, most authors generally reported normal scale effects on joint strength (represented by negative exponential regressions). However, there were also rare exceptions (Swan & Zongqi, 1985; Kutter & Otto, 1990; Giani *et al.*, 1992).

In essence, whether scale effects are normal or inverse is of great importance in assessing the significance of data drawn from small samples testing, which may be very serious when safety of civil and mining works depends on a correct assessment of field conditions. If the scale effect is inverse, data from small samples are on the engineering safe side; if it is normal, they become against workings safety.

However, the problem is not that simple because lithological, morphological and mechanical conditions of small samples are not comparable to those of large samples due to sampling biases. This means that individual small samples cannot represent the weathered and crushed zones of large ones. On the other hand, large discontinuities in nature are commonly mismatched, because shear displacements are more frequent as the joint dimensions increase (Leal Gomes, 1999a), so this fact favours the appearance of normal scale effects. Besides, the undulations of large matched discontinuities have larger amplitudes than those of small samples, where sometimes only the smaller roughnesses are present. But the amplitudes of undulation or roughness provide a favourable contribution to joint strength which is not foreseen by any limit equilibrium model, like Patton's model (Patton, 1966).

Therefore, the problem under analysis is a complex one (Leal Gomes, 2000) for it is necessary to observe many features: the matching or mismatching of rock discontinuities, the presence of weathered and crushed zones, sampling biases, the characteristics of the undulation and roughness of the walls, the test conditions and other aspects that strongly constrain the estimation of the scale effect on the joint mechanical parameters.

In order to understand the integrated behaviour of those multiple effects, numerous experimental tests on samples from a large artificial joint existing in a porphyritic granite from Pontido (Vila Pouca de Aguiar, Portugal) were carried out. They helped to devise the achievement of sev-

Manuel J.A. Leal Gomes, Associate Professor, University of Trás-os-Montes e Alto Douro, UTAD, Vila Real, Portugal. e-mail: mlgomes@utad.pt.
Carlos Dinis da Gama, Full Professor, IST, Technical University of Lisbon, Portugal. e-mail: dgama@ist.utl.pt.
Submitted on February 14, 2008; Final Acceptance on March 2, 2009; Discussion open until April 30, 2009.

eral assertions and essential conclusions in the domain of rock mass joint mechanics.

2. Choice of Test Material

The greatest difficulty in rock discontinuity testing is the acquisition of a sufficient number of samples to obtain representative data, as it is often necessary to reuse the same sample several times in laboratory mechanical tests. During each test there is wearing of sample walls and due to that, successively obtained data are not rigorously based on the same initial test material, which brings about serious interpretation problems.

Bandis (1980) used sample casts in synthetic material of a natural joint but the difficulties of this procedure are well known, for they include the fitting of sample properties to the similarity conditions given by dimensional analysis and the physical acquisition of samples in good conditions. Bandis himself refers to the mismatching ("rocking") of their synthetic samples, which surely had a great influence on their conclusions, as it will be observed. Gracelli (2001) also used casts in synthetic material but not referring the similarity conditions. On the other hand, his experimental study was not dedicated to scale problem analysis, like Bandis' thesis and this paper, which involve other types of questions.

Barton & Choubey (1977) assert that the testing of ten samples having the same size provides reliable strength averages for those dimensions. Harrison & Goodfellow (1993) studying discontinuity roughnesses in granites with Renger discs (Brown, 1981) concluded that their scale effect disappeared for sample dimensions larger than 25 cm x 25 cm. However, the variation of parameters describing roughness (considered the most important factor on scale effect studies of joint strengths at the dilating phase of slides), is mainly due to the resultant vector of normal directions to the discs and of the roughness anisotropy, and cease to be important from a REV around 250 cm^2 (16 cm x 16 cm) of roughness and anisotropy (Leal Gomes, 1998).

The opening of an artificial discontinuity, by introducing chisels in a large block of porphyritic granite having 2.7 x 1.6 x 1.5 m^3 in volume was decided, in an attempt to contribute to the clarification of these matters. These dimensions are close to the sizes of the natural blocks observed near the surface of the Pontido batholith and that artificial joint in particular had about 4.32 m^2 in area. Artificial discontinuities are different from the natural ones because of their better matching, higher roughness, absence of wall weathering and lower hydraulic conductivity (Gale, 1993).

The following samples corresponding to the maximum possible utilization of the available material were extracted: 8 square samples type I (16 x 16 cm^2), 8 rectangular samples type II (16 x 10.7 cm^2), 9 samples type III (16 x 8 cm^2), 9 samples type IV (16 x 5.3 cm^2) and 5 samples type V (10.5 x 8 cm^2). This number of samples is lower than that recommended by Barton & Choubey (1977) but they are still significant, as the small scattering of data shows.

3. Morphology of the Discontinuity Samples

The discontinuity walls of these samples were sound, rough and well mated, having an average *JCS* (joint compressive strength) of 115.4 MPa and a residual friction angle (φ) of 28°, obtained in pull tests with completely smooth and plane surfaces. The rock had an average density of 2.72 g/cm^3 and a Young modulus of 59 GPa, obtained on prismatic samples having 6 cm x 6 cm x 15 cm. It had feldspar megacrystals, up to 2 cm in length, in a quartz, biothite and clorhite matrix.

All the samples were photographed under oblique light, which accentuates the wall relief and roughness, as well as contrasts between crests and valleys. After this operation the contour profiles of all the sample walls were outlined on white paper using a pencil and the corresponding *JRC* was estimated through comparison with the Barton & Choubey (1977) typical profiles.

Prior to testing, prints in smooth tracing paper were made of the actual contact areas between the sample walls in their best fit positions, under an average normal stress in the joint (σ_n) of 10 kPa (before pull tests) and 1.2 MPa (before tests in the sliding machine). The prints were produced by using thin sheets of blue dentist paper introduced with smooth tracing paper between the joint walls. The obtained spots were analysed through image processing by scanning the prints at 400 DPI and leading to histograms of different grey levels. This method proved to be sufficiently objective to allow general quantitative conclusions, while the other referred methods only provided qualitative ideas on sample roughness.

4. Sample Roughnesses

Averages and dispersions of *JRC* parameters obtained through comparison between sample walls and the typical profiles of Barton & Choubey (1977), varying between 8 and 16, did not exhibited scale effects. The main reason for this fact is the great subjectivity of these comparisons, as it was demonstrated by a tendency to focus on the more abrupt aspects of the profiles and of the wall surfaces (Leal Gomes, 1998), which increases the *JRC* obtained by comparisons. On the other hand, the amplification and the reduction of the typical profiles, in order to make those comparisons among profiles of different lengths, is quite invalid. These *JRC* obtained by visual comparison only have a morphological content. In fact, the typical profiles of Barton & Choubey (1977) were obtained by outlining the profiles of their original joint samples, followed by performing pull tests and attributing to them the *JRC* deduced from Barton's model (1990):

$$JRC = \frac{\tan^{-1}\left(\frac{\tau}{\sigma_n}\right) - \varphi}{\log\left(\frac{JCS}{\sigma_n}\right)} \quad (1)$$

where τ is the peak shear strength.

Therefore, these *JRC* are experimental and have not only morphological meaning but also mechanical contents and are not only roughness parameters but also strength properties. For instance, the experimental *JRC* also depends on the amplitude of roughness, as the typical profiles of Barton & Choubey (1977) demonstrate, increasing their *JRC* as the amplitude of profiles increase. Besides, the mental amplification and reduction of profiles is based on an erroneous principle, asserting that rigorously homothetical changes with the scale of roughness of the original samples of Barton & Choubey (1977) does not change their *JRC*.

This assertion needs experimental demonstration and probably is wrong. Such comparisons also outlook the differences between *JCS* and σ_n of the original samples of Barton & Choubey and the *JCS* and σ_n of the other samples and discontinuities taken in the field. Therefore, the values of *JRC* estimated by comparison only have a geometrical content and so deducting strength parameters from them is not correct.

In this study, *JRC* data obtained by comparison did not detect either the obvious anisotropy in the samples direction, which is visible through the drawing of the sample contours (Fig. 1) or the smaller anisotropy of orientation (for instance, NS direction has two possible orientations, NS and SN), which was shown by subsequent pull tests.

The data distribution of the maximum amplitudes of roughness (R_{max}), which were measured between the highest crest of a sample wall and its deepest valley, suggests not only the increasing of R_{max} as the larger linear dimension of the sample increases, but also that R_{max} does not depend on the smaller sample dimension (Table 1). For instance, the values of average and maximum R_{max} are clearly lower in samples of type V (size 10.5 cm x 8 cm) than in other sample types where differences on R_{max} are nearly always smaller.

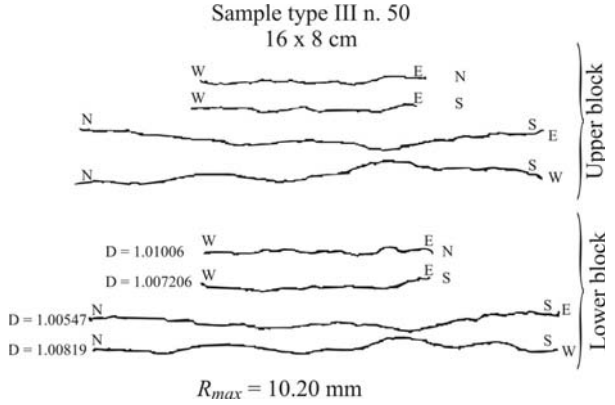

Figure 1 - Contour profiles of sample type III n. 5D.

But the most important information given by the outline of the sample wall contours was the clear image of shorter dimensions, showing lower roughness values than larger ones, which is contrary to the assertions of most authors (Cunha,1990; Barton, 1990; Bandis, 1990; Pistone, 1990; Maerz & Franklin, 1990), who usually assert that smaller lengths have larger roughness magnitudes.

5. The Problem of Sample Roughness

Patton's model (Patton 1966) asserts that the joint strength in the dilating phase of rock joint sliding is given by:

$$\tau = \sigma_n \tan(\varphi + i) \quad (2)$$

where *i* is the dilation angle given by the slope of joint asperities. Patton checked experimentally this equation for low normal stresses σ_n.

At UTAD, a series of pull tests were conducted under a σ_n of 0.6 kPa on moulded discontinuities made with Portland cement mortars and river sand. These discontinuities had homothetical triangular asperities presenting slopes around 20°, 30°, 45° and 60° as well as different heights or amplitudes (h) of 0.6, 1.2, 1.8 and 2.4 cm (Fig. 2). Upon the shear testing, Patton's model was verified, except for some slight fluctuations of shear forces attributable to effects of spurious momentums developed during slidings which are not foreseen by Eq. (2)).

Therefore, τ depends on *i* and not on h for regular asperities. However, when the work done by shear forces involved in slides is considered, it was observed that it changes for the same *i* as h increases. Actually, the strengths of these joints having the same *i* but different h are not rigorously described by shear forces but by the strain energies needed for sliding. These energies cannot be measured in the laboratory or in field but may be roughly calculated, so adequate representation of real joint strengths in the dilation phase is not possible.

However, this dilemma probably is mitigated by the less schematic conditions of the asperities in natural discontinuities. A sudden upper wall sliding was observed

Table 1 - Maximum amplitudes of roughness.

Sample type (cm^2)	R_{max} (mm)		
	Average	Maximum	Minimum
I - 16x16	10.72	14.5	8.3
II - 16x10.7	12.72	16.85	10.9
III - 16x8	10.59	15.3	8.3
IV - 16x5.3	10.71	13.3	8.05
V - 10.5x8	9.37	11.5	8.3

(Leal Gomes 1998) in pull tests on samples from the large artificial joint previously mentioned, when having imbricated asperities and several roughness levels (roughness levels are undulations having the same amplitude but either different wave-lengths, or their crests shifted from each other). In the tests with regular homothetical teeth mentioned above, the overcoming by the upper wall of regular asperities was a gradual one.

Therefore, in natural matched discontinuities having irregular asperities with different i, h and morphologies, the amplitude of roughness in the dilating phase has probably implications on the peak shear force, which is accumulated against the asperity faces until their sudden yielding (Leal Gomes 2000; Gracelli 2001). In that case, the higher the asperities are, the larger is the shear force. Therefore, for the same σ_n and morphological *i* (but different h) there are different values of tan (φ + *i*) and *i* deduced from Patton's model values, so the linear dimensions of amplitude are transformed into dimensionless increases of the dilation angle, and the asperity amplitudes are taken into account by variations of dilation without morphological correspondence.

The above mentioned dilemma is solved, although with loss of physical information, however, intermediate behaviours of difficult evaluation are possible. This approach still demands a better experimental verification, but this principle may be checked with the typical profiles of Barton & Choubey (1977) where higher *JRC* corresponds to profiles having higher amplitudes. These *JRC*, like the experimental *JRC* of this paper, were experimentally deduced from Eq. (1) of Barton's model.

This assertion was presented to point out the use of linear dimensions, like R_{max}, for representing joint strength and not dimensionless parameters, as it is done usually. At present, no strength model includes these linear parameters, including recent approaches such as that of Gracelli's model (Gracelli 2001).

Thus, it was demonstrated that small samples have lower roughness than larger ones, quite the opposite to what usually is admitted by most authors, if and when the middle plane of all samples is levelled. Furthermore, small samples must have necessarily lower roughness than large ones (from the same joint) because the linear parameters related to asperity amplitudes - such as R_{max}, or the average of distances to middle line (CLA), or the standard deviations of roughness amplitudes, RMS (Muralha 1995) or even the dimensionless roughness parameters, like Z_2 (Tse & Cruden 1979), dilation angle (*i*), R_p (quotient between the length of a profile and its middle line length (Sage *et al.* 1979) and D (fractal dimension) - diminish as the middle planes of smaller and smaller samples are levelled. In Gracelli's model (Gracelli 2001), the parameter A_c which is the potential contact area ratio for a threshold dip angle of asperities is given by:

$$A_c = A_0 \left(\frac{\theta^*_{max} - \theta^*}{\theta^*_{max}} \right)^c \qquad (3)$$

where A_0 is the maximum possible contact area of the joint walls, θ^* the apparent dip inclination of asperities, θ^*_{max} the maximum apparent dip angle in the shear direction and *c* a roughness parameter calculated using a best fit function, which characterizes the distribution of apparent dip angles over the surface, also denote a roughness reduction as smaller and smaller samples are levelled.

Figure 3 demonstrates that the division of a large sample into small samples, accompanied by their systematic levelling, reduces R_{max} on each small sample with reference to the large sample. And it is easily understood that reducing the asperity slopes in a large sample by dividing it into small samples, which are systematically levelled, if the samples are systematically subdivided into very small dimensions and the middle planes of all samples are levelled, in the limit, as areas tend to zero, leads to obtaining horizontal joint surfaces. To the contrary, in the limit one shall have almost vertical surfaces with the traditional procedure, *i.e.*, by leaving the middle plane position at random.

This is obviously the result of a roughness idea that is very close to a mechanical conception of the problem, where indices like amplitude, wave-length roughness, undulation and asperities slopes are very important. The laboratory tests on matched samples are thus on the safe side of engineering in the dilating phase of slides with reference to the large original natural matched discontinuities, whenever all of them are levelled.

With this procedure, the mechanical and morphological aspects connected with asperity slopes are also affected by subdividing and levelling of samples, resulting in lower morphological indices, lower average dilation angles and even lower *JRC* deduced from Barton's model.

So, previous conceptions may need revision where only the morphological aspects connected with asperity slopes prevail, like the calculation of *JRC* from a fractal dimension (D). Actually, Fig. 1 shows that shorter profiles of

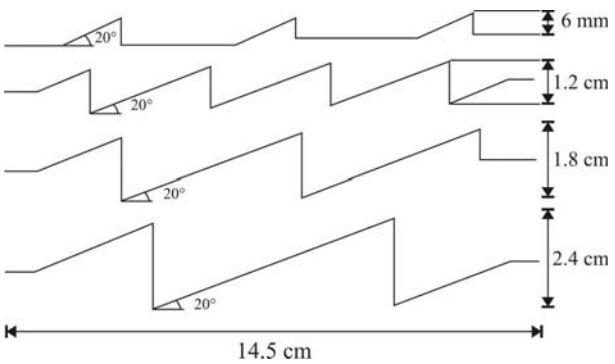

Figure 2 - Regular profiles having homothetical teeth with slope of 20° and amplitudes of 0.6, 1.2, 1,8 and 2,4 cm tested by the authors in UTAD.

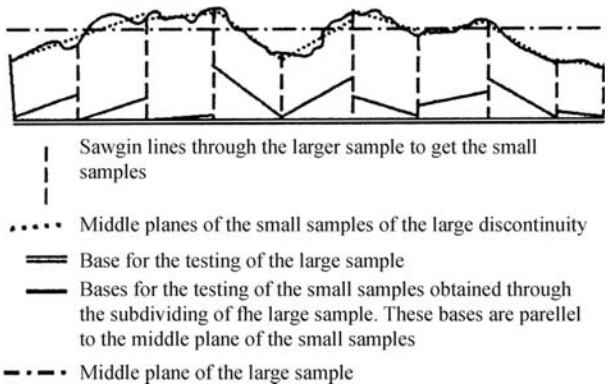

Figure 3 - Subdivision of one large sample into nine small samples and systematic levelling of their middle planes.

the samples 5D seem to have higher fractal dimensions but lower roughness, contradicting the well known statistical regressions such as:

$$JRC = 1000\,(D - 1) \qquad (4)$$

For instance, in the direction of the larger contour profiles of the rectangular sample 5D, the experimental value of *JRC* is 10, but in the direction of the shorter profiles it is only 8, but a different *JRC* obtained from the experiments is deduced from Eq. (4).

In Fig. 1, the greater amplitude of roughness of the larger profiles favouring the strength is observed. Actually, these regressions equations like 4) are supported by a traditional view of scale effects on joint strength, involving strength reduction as sample sizes increase and this perspective is supported by tests on mismatched samples. This fact completely changes the scope of considerations by Bandis (1980), who refers the mismatching of their synthetic samples. The model of Peres Rodrigues & Charrua Graça (1985) would be more adequate for them, but not Patton's model. It is remarked that Peres Rodrigues & Charrua Graça's model implies normal scale effects, which are precisely due to sample mismatches.

Hencher *et al.* (1993) repeated Bandis tests on the same synthetic material but they found a scale effect having a maximum value for intermediate dimensions, probably because they did not level the samples and tested different combinations, up slope and down slope, of middle positions of joint samples. The importance of this aspect is more serious when the discontinuity is rougher, because it is equivalent to either add or subtract from *i* a spurious angle which seriously influences higher tan ($\varphi + i$).

Besides that, the partition of a sample is a highly arbitrary operation, as Fig. 4 demonstrates, where only the s surfaces resist, if the larger a) sample is tested from North to South. When that sample is broken in five smaller volumes b), the u surfaces will also be tested and the resulting spurious results will affect the average strength values, which are much different from those of a). At u there is a spurious shear component of σ_n favouring the sliding.

In samples taken from natural discontinuities there are roughnesses and undulations of several ranks or orders that are characterized by their different amplitudes. The lower amplitude is the first order one, having roughnesses and undulations of higher order as h increases. It is more probable to have undulations of higher amplitudes with larger samples, whose slides require greater applied shear forces. It is also still necessary to consider different roughness levels and different types or shapes of asperities.

Therefore, the observation of a discontinuity roughness is a complex task. On this account, to cut a sample off may correspond to the removal of some orders, levels or types of roughness, as Fig. 5 indicates, where AA divides a larger sample into smaller samples having different anisotropy of orientation from the original sample context and where levels and types of roughness were removed with important mechanical consequences.

Bandis (1980) demonstrated that the actual contact areas between joint walls are larger and more distant in large samples, which have larger empty spaces. With small samples the contacts are smaller and more scattered. With samples of the artificial joint removed from the Pontido granite block, it was observed that the percentage of actual contact area (Aef), obtained in accordance with section 3, with reference to the total sample area (Aa or Area) is greater in small samples than in large samples (Leal Gomes 1998, Fig. 6). Therefore, the actual stresses in real contacts between walls (Sigef = σ_n.Aa/Aef) are higher in larger

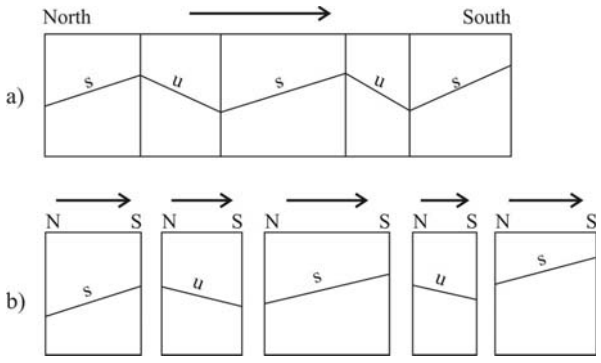

Figure 4 - Conceptual experience about the arbitrariness of subdividing a large sample into small samples.

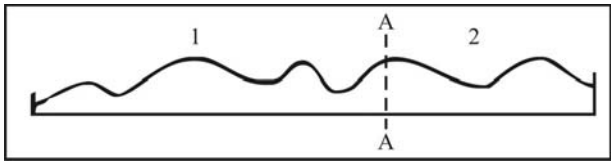

Figure 5 - Division of a sample in accordance with AA into two smaller an asymmetrical samples.

samples, but this difference diminishes as σ_n increases because the bending of walls on larger empty spaces in large samples, bringing their walls in contact and thus increasing Aef, which is easier in those large samples rather than in small samples. In spite of the low correlation coefficients *R* in the Aa vs. (Aef/Aa) plotting, the original variation of Aa *vs.* Aef had $R = 0.48$ (for σ_n of 10 kPa) and 0.66 (for σ_n of 1.2 MPa).

Gracelli (2001) found actual contact areas between their joint sample walls very much higher than those of Fig. 6 (up to 70% or more in fresh tensile joints). Their joint sample walls had an almost perfect matching because they were obtained into small prisms of rock having transverse areas of tens of cm^2, while the samples of the present experimental study were withdrawn from a large artificial discontinuity having 4.32 m^2, created from a 2.7 x 1.6 x 1.5 m^3 granite block. Leal Gomes (2001b) demonstrates that to obtain this joint in the vicinity where the rupture surface passes following the rock imperfections is much greater for the larger volumes of rock than for smaller ones, leaving a great amount of dust and rock fragments between walls in the first case to the detriment of their matching, which does not happen in smaller rock volumes. On the other hand, the features which control the rupture during the production of natural joints are different at two different scales. Therefore, the roughness patterns obtained either in great or in small rock blocks and their morphologies are of difficult correlation.

Concisely, an expeditious observation of the facts demonstrates that the artificial joint samples of Pontido have essentially only one roughness order, with an amplitude around 1 cm and smaller asperities swinging around this roughness. It was verified that sample areas were large enough to contain the greater amplitude of roughness in the whole 4.32 m^2 original artificial discontinuity. Therefore,

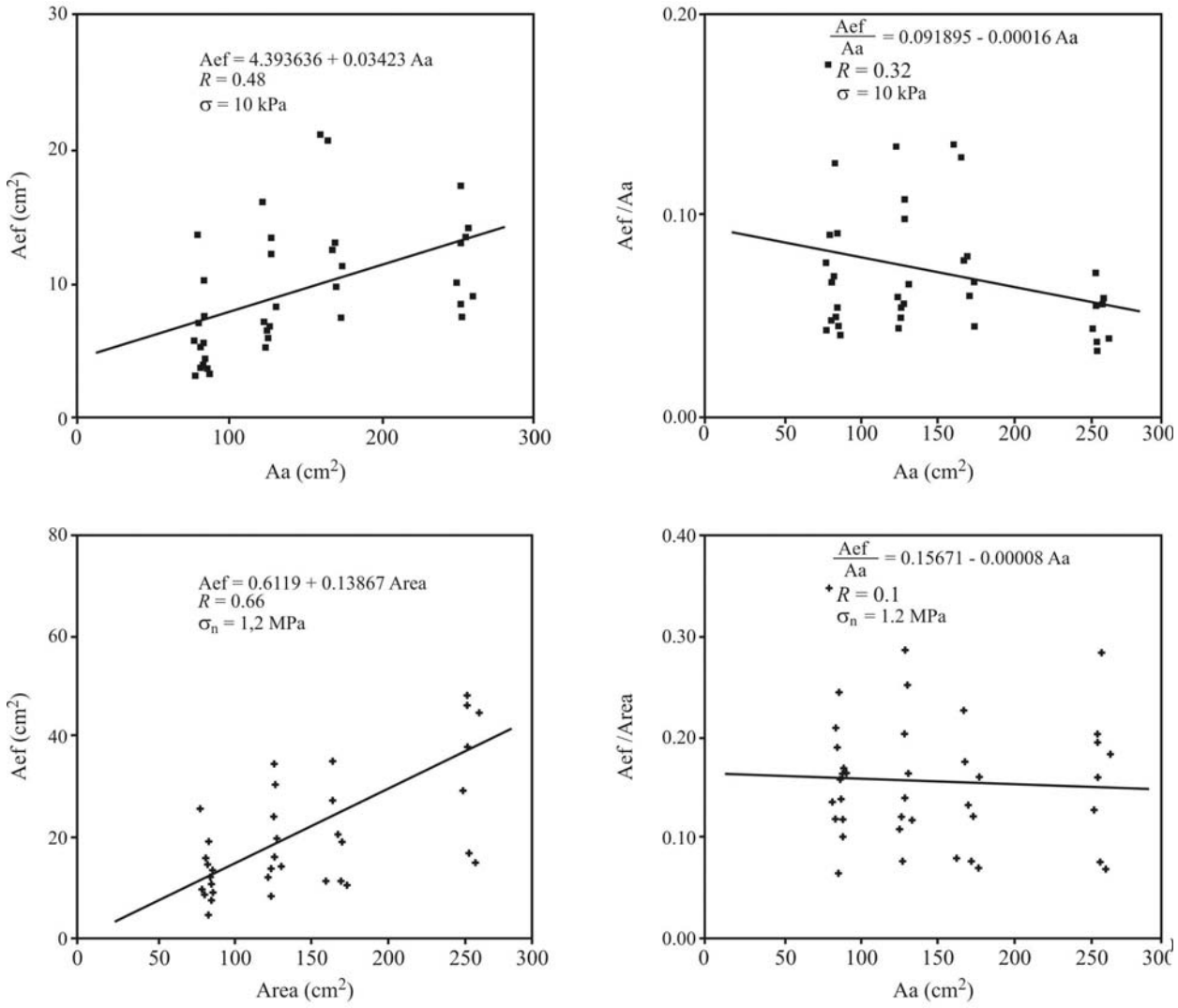

Figure 6 - Graphics (Aa x Aef) and (Aa x (Aef / Aa) for σ_n of 10 kPa and 1.2 MPa. *R* is the correlation coefficient.

an area of 16 cm x 16 cm is probably close to the roughness REV for this artificial discontinuity in granite, as suggested by Harrison & Goodfellow (1993).

6. Pull and Sliding Machine Tests

A total of 1200 pull tests on those joint samples loaded under σ_n of 1 kPa were carried out in two directions, both parallel to the rectangular contour edges. The NS direction was always parallel to their larger dimension (usually 16 cm and 10.5 cm at samples type V) and the EW direction was perpendicular to it. Samples were tested in accordance with NS and SN orientations at the NS direction, and WE and EW orientations at the EW direction. The middle plane of all the joint samples was previously levelled before each test in accordance with the two discontinuity sample lower wall diagonals (Fig. 7). At least three pull tests were carried out for each orientation of each sample, under the weight of the upper block (Fig. 8). The wears in these tests were insignificant or non-existent. The traction wire and the belt around the upper block also were levelled and placed just over the level of the higher protuberance of the sample contour to avoid, as far as possible, inconvenient force momentums.

During the tests it was verified that a lack of attention to these details caused errors of up to 40% with respect to test data obtained correctly. The slides in pull tests were sudden, without meaningful premonitory movements.

The same samples were settled into cement mortar blocks for additional tests in a shearing machine in accordance with SN orientation, after adequate levelling, under σ_n of 0.05, 0.3, 0.6 and 1.2 MPa.

Barton & Choubey (1977) assert that a shear displacement of 1% of the sample length usually was necessary to reach peak conditions. Total displacements of 6 mm under the last σ_n level of 1.2 MPa trebled the recommended value to enable comparison among samples after their final wears were reached. Under lower σ_n levels, the displacements were halted as soon as the peak conditions were reached, preventing excessive wears of joint sample surfaces.

The wears caused by the tests with the sliding machine were assessed through new pull tests in accordance with all orientations (NS, SN, WE and EW). It was verified that at SN orientation a strength loss of 70% occurred with a loss of 40% for *JRC*, but strength and roughness were reasonably preserved in accordance with the other orientations (Fig. 9). For instance, at WE orientation, 5.3 cm type IV samples maintained 93% of their original *JRC*, so they were also tested in the sliding machine under the same σ_n levels of 0.05, 0.3, 0.6 and 1.2 MPa, in accordance with this WE orientation to check tendencies of scale effects (Fig. 10).

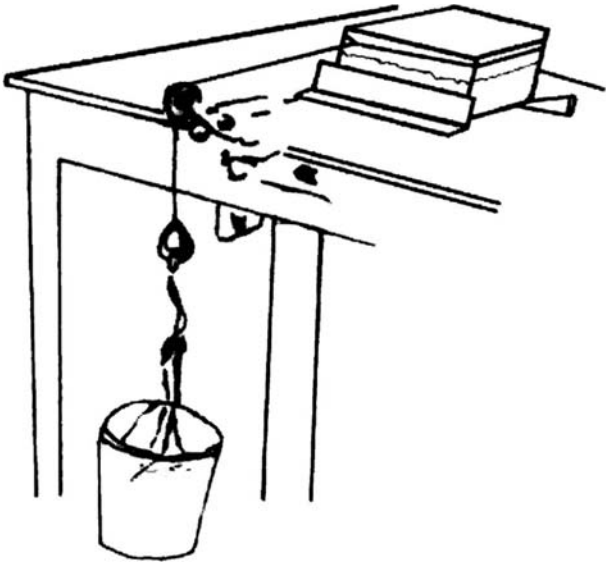

Figure 8 - Pull test apparatus. The sliding of upper block was caused pouring lead grains into the bucket.

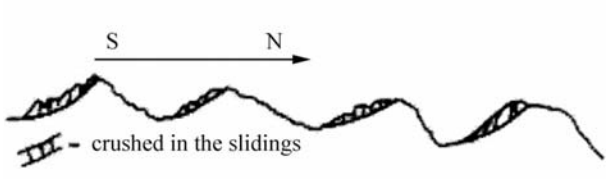

Figure 9 - Damage of roughness in shearing machine at SN orientation, but preservation of roughness in agreement with other orientations.

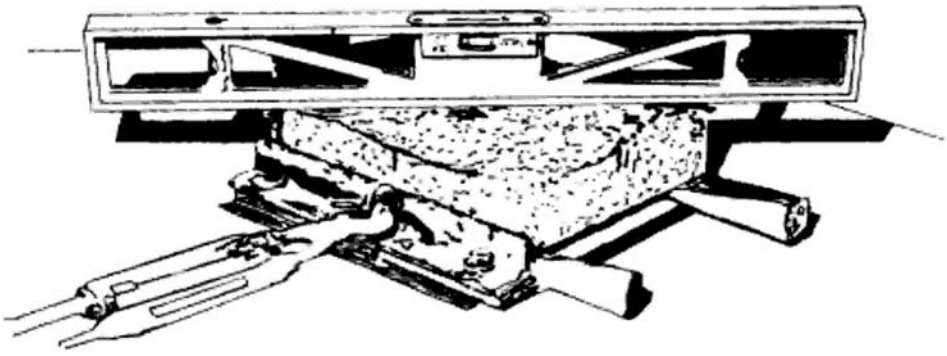

Figure 7 - The levelling of the middle plane of the samples was made with a level introducing wedges under the lower block.

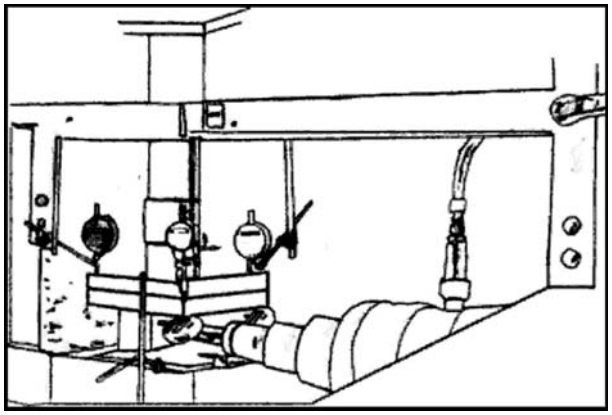

Figure 10 - Sample type IV assembled into the shear machine for a WE shear test.

7. Test Data

In pull tests, the predominance of inverse scale effects was observed when Barton's model was used. Data of Fig. 11 show the increase of roughness and strength at EW direction (WE orientation plus EW orientation) as sample areas (Aa) and lengths increase.

Figure 12 refers to pull tests at SN direction as the transverse dimension to slides (or widths) increase. A slight normal scale effect was observed, but the correlation coefficient *R* was very low. The Student correlation test for 95% of confidence demonstrates that the resulting correlation is random and was not due to a genuine scale effect.

Figure 13 contains all pull test data at the four stipulated orientations including the sample type V values and a clear inverse scale effect is observed.

Figure 14 shows the decrease of anisotropy of direction which tends to zero as sample areas and symmetry increase. The REV of this anisotropy is reached for 16 cm x 16 cm dimensions in these pull tests.

Figure 15 (a) represents the anisotropy of orientation (*JRC* NS - *JRC* SN) along the NS direction. Figure 15 (b) shows the anisotropy of orientation (*JRC* WE - *JRC* EW) for the WE direction. Figure 16 presents the evolution of the average of these two anisotropies of orientation.

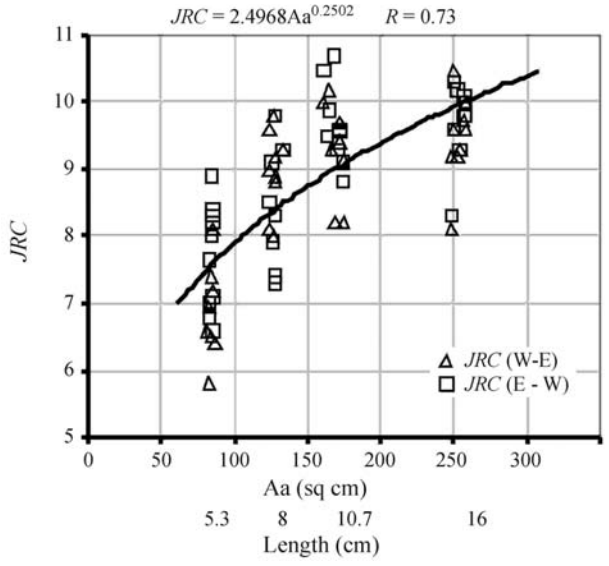

Figure 11 - Graph ((Aa and length) x (*JRC* (EW). Sample widths of 16 cm.

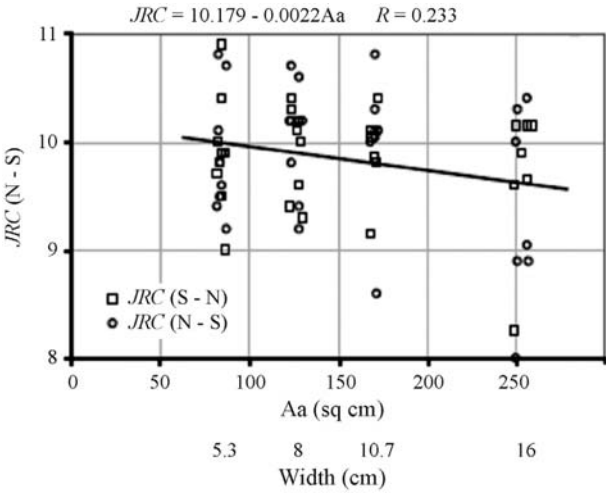

Figure 12 - Graph ((Aa x *JRC* (NS)). Sample lengths of 16 cm.

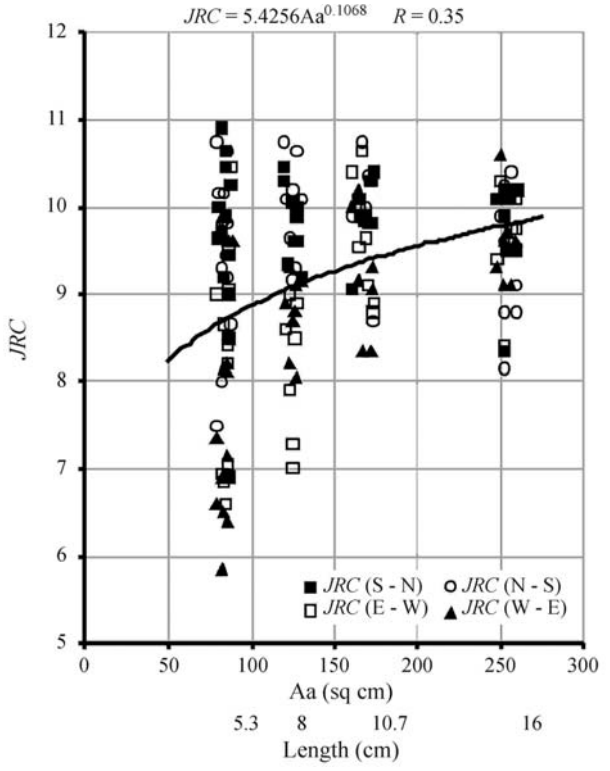

Figure 13 - Graph (Area x *JRC* (NS direction plus EW direction of all the samples)). The graph includes samples type V.

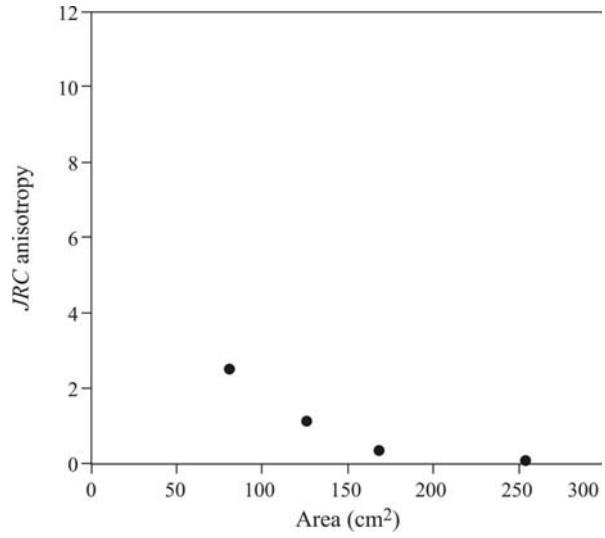

Figure 14 - Graph (Area x (*JRC* NS - *JRC* EW)). Anisotropy of direction of *JRC*.

These last diagrams also show the reduction of anisotropies of orientation as sample dimensions and symmetry increase. Unlike the anisotropy of direction, their REV are not zero, remaining around 0.5 *JRC* units for areas larger than 250 cm^2.

Figure 17 refers to sample shear tests at SN orientation under σ_n levels of 0.05, 0.3, 0.6 and 1.2 MPa. The reduction of peak shear strength (τ) as the transverse dimension to sliding direction (the perpendicular widths) increases from 5.3 up to 16 cm is observed. These normal scale effects are accentuated as σ_n increases.

In spite of the low correlation coefficient in the curve corresponding to 0.3 MPa, the correlation coefficients of the other curves are moderate and this graph suggests the close dependence of shear strength on the width of tested samples.

Muralha & Cunha (1990), whose joint samples were obtained in schistose rock probably with lower *JRC* and

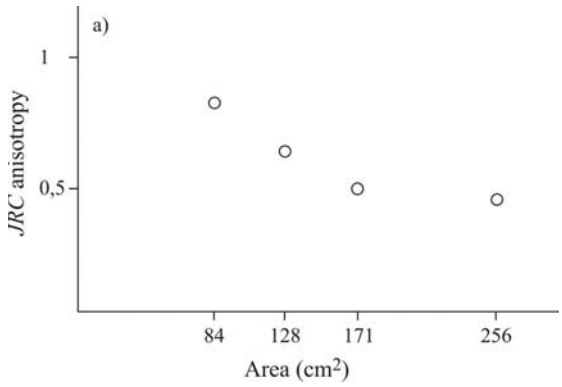

Figure 16 - Evolution of (*JRC* EW anisotropy + *JRC* NS anisotropy)/2.

JCS than the present samples, did not obtain this τ dependence on the widths. These facts seem to point out the increase of this effect of sample width on the shear strength as *JRC*, *JCS* and σ_n increase.

Lower strength for worn samples type IV at WE orientation than at SN orientation, were found in the sliding machine tests. Inverse scale effects probably tend to vanish as σ_n increases, but these tendencies are not clear and explained.

The shear machine was not very rigid, so gauge readings near peak conditions were difficult to obtain. The peculiar shape of the samples may cause some suspicions of spurious influences on data because of shape effects, but this preoccupation is unsubstantiated. The adoption of these unusual sample shapes actually brought out some behaviour types, facilitating the interpretation of the phenomena, without loss of generality.

8. Discussion of Scale Effects on Rock Joint Strength in Accordance with the Experimental Work

It was already observed the decreasing of joint roughness as sample sizes diminish by cutting them when the

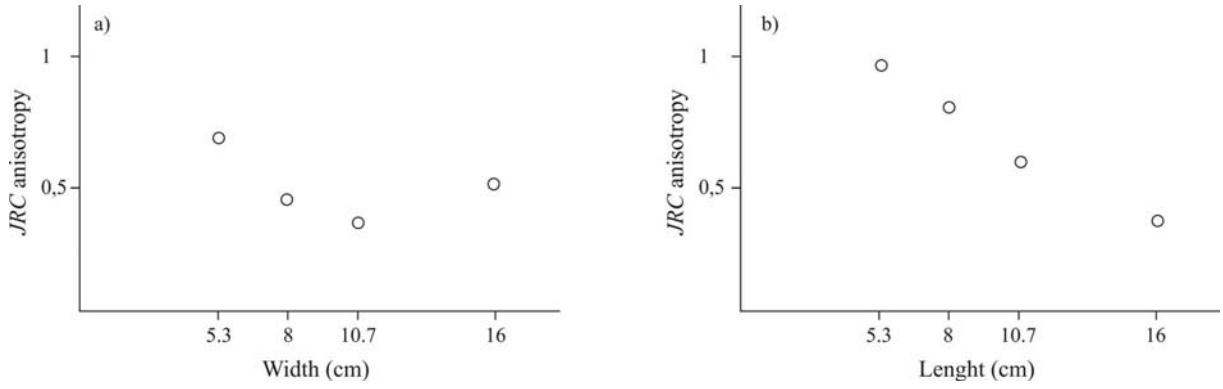

Figure 15 - Anisotropy of orientation of *JRC* at NS direction (sample length of 16 cm); b) Anisotropy of *JRC* for the EW direction (sample width of 16 cm).

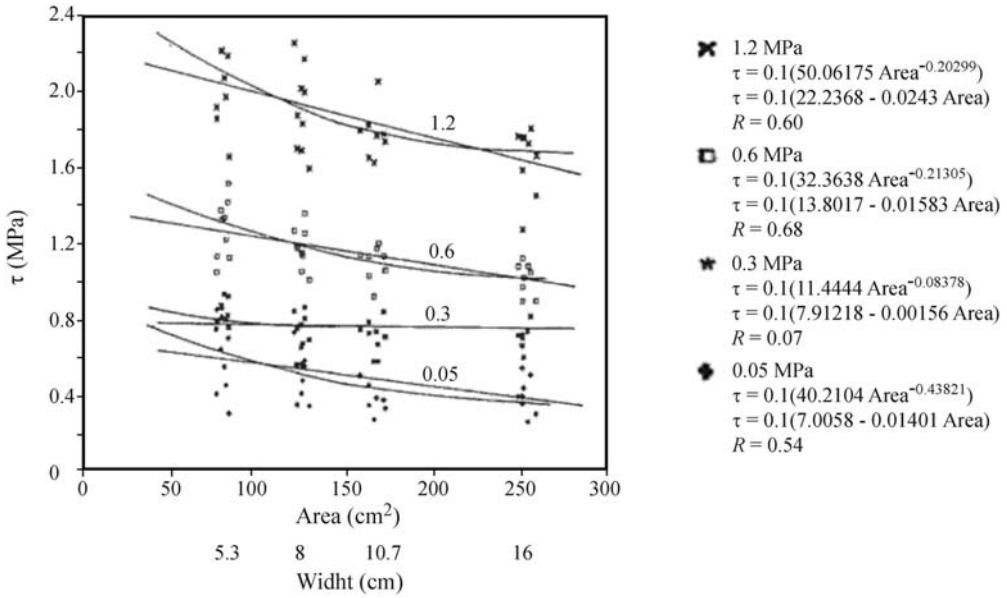

Figure 17 - (Area and width x τ) for s_n of 0.05, 0.3, 0.6 and 1.2 MPa. Sample length of 16 cm.

middle plane is levelled. At the dilating phase of the slidings, if the roughness was reduced the sample strength also decreased. Apart from this reason for the appearance of inverse scale effects in these tests, there are two other possible complementary mechanisms having the same effect. Actually, it is possible that φ will diminish as σ_n tends to zero, contrary to Patton's (1966) assumption, such as for very high σ_n, as σ_n increases. Basic friction angle of silicate rocks may decrease to 10° as σ_n tends to zero (Hencher *et al.*, 1993), while for mid σ_n, φ remains around 30°. The gathered test data about this matter show a great scattering but that possibility is not discarded. The ignorance of φ evolution as σ_n tends to zero, may only be understood because this vicinity is hardly involved in real geotechnical problems. The dilation contribution in this same vicinity may not exist or be lower than *i* but it is only completely mobilized when there is a minimum value of σ_n.

An increasing τ / σ_n (and not a constant one) for low σ_n values was admitted (Leal Gomes, 1999b), contrary to Patton's model. Figure 6 suggests higher Sigef in larger samples becoming greater (Sigef.(Aef / Aa) . tan (φ + *i*)), that is, the shear strength. This mechanism should lose its importance as σ_n increases (Fig. 6) because the slope of the diagram Aa vs. (Aef / Aa) and therefore of Aa vs. Sigef values is reduced for high σ_n values, when another evolution for tan(φ + *i*) appears.

The other complementary mechanism is less controversial and supported on the knowledge of the average peak displacements (d_p) obtained in tests under a σ_n level of 0.05 MPa (Table 2).

The mean shear strengths are not exactly inversely proportional to d_p. They show otherwise a clear inverse magnitude order with respect to d_p and by analysing the curved paths of the top block (assuming they are circular) they show a small average curvature radius C = 0.139 m. This is valid under the condition that such a radius C path is observed when the sample's top border overthrow the lower border asperities, in the type IV samples along the WE edge, which is smaller (5.3 cm size) than the SN edge (16 cm size).

The sliding of samples type I (16 cm) was done with a C of 3.869 m and samples type IV slides at SN orientation (16 cm) with the largest C of 5.028 m. This analysis was performed upon the readings in gauges.

Actually, the upper block in longer samples needs to overcome the whole asperity heights in its translating movement, whereas, despite our samples being mated, a rounder movement of the upper block over the asperities occurred in short samples, like WE orientation of samples type IV, causing larger peak displacements but lower strengths. Samples of type I, which are wider, show greater d_p and lower τ than samples type IV at SN orientation, due to their greater wealth in roughness levels, which becomes rounder the overcoming of asperities.

Actually, Fig. 18 shows the increase of general roughness symmetry and reduction of anisotropy as two or more

Table 2 - Average peak displacements (d_p) and average curvature radius (C) of upper block sliding trajectories.

Sample (cm^2)	Orientation	dp (mm)	τ (MPa)	C (m)
16 x 5.3	SN (16 cm)	0.19	0.6	5.028
16 x 16	SN (16 cm)	0.24	0.46	3.869
5.3 x 16	WE (5.3 cm)	0.6	0.2	0.139

roughness levels are laterally juxtaposed, indicating that the larger the samples, the greater are the number of these juxtapositions. Due to this effect, the anisotropy of mated samples decreases in Figs. 14, 15 and 16 as sample sizes increase, and the slides are rounder, having lower strength as the transverse dimension to sliding, that is, the sample widths, vary from 5.3 to 16 cm.

Due to all these reasons, in the dilating phase of slides, sound, fresh and mated discontinuities must have inverse scale effects, vanishing as σ_n increases, because then the dilating character of slides, which begin to occur with asperity cut, is lost.

However, there are not reasons to admit *a priori* that scale effects on joint strength become normal ones only because the scale effect on *JCS* is eventually normal. That fact has little influence, because the differences among transverse dimensions of asperities to be cut are not important enough, either in large or in small samples. Besides, it is necessary to bear in mind that the measured scale effects on uniaxial compression strength of some rocks, mainly porphyritic like Pontido granite, are inverse (Leal Gomes, 2001a).

It is deduced from this exposition that, if discontinuities are well-mated, the average slopes of different roughness levels must be added to reach their strength, so the roughness slope i_1 swinging around the undulation of higher order must be added to its slope i_2 and the corresponding factor in Patton's model is given by tan ($\varphi + i_1 + i_2 + ...$).

Thus, large samples having higher undulation orders, must have greater strengths than small ones, where there only exists small roughness. Therefore, these small samples are on the safe side of engineering. Besides, there is the amplitude of the undulation effect, not foreseen by Patton's model favouring the large sample strengths, where several undulations of higher amplitude may be found. Clear inverse scale effects on τ of matched discontinuities (and these samples of the 4.32 m^2 artificial joint of Pontido are matched) result from these facts. However, the panorama is rather different when the discontinuities are mismatched, as in the Bandis (1980) samples (Fig. 19), because of the imbrications of small asperities, which do not partially or wholly intervene in slides cannot be taken into account. In this case, the consideration of only the average slope of large undulations is necessary, which is usually gentler than roughness slopes. On the other hand, contributions of amplitude will also be much reduced with reference to a situation of complete matching, since the walls are shifted to each other. Peres Rodrigues & Charrua Graça's model (1985) is the appropriate model for these conditions, not Patton's. An extremity of the upper wall of the samples leans on the lower wall and the upper wall turns around the more conspicuous asperity, that is, the irregularity being the hardest to overcome, that is named as the meaningful irregularity for that model.

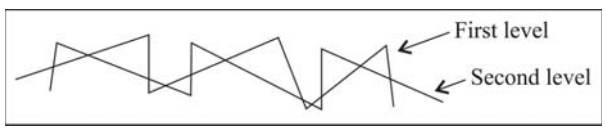

Figure 18 - Two different roughness levels laterally juxtaposed increased the symmetry of the sample.

Figure 19 - Mismatched joint. The roughness slope is i_1, the undulation slope is i_2, the amplitude of undulation is a_1 and the amplitude contribution for strength at a mismatched discontinuity is only a_2.

Contrary to Patton's model, in Peres Rodrigues & Charrua Graça's model the movement of upper wall is not parallel to the lower wall and dilation angles are clearly lower than in Patton's model. These two authors postulated that the median of heights of that meaningful irregularity (H) relates to the sample area (A) in accordance with a function ln$A(H^2)$. If L is the sample length and the distribution of the meaningful irregularity is uniform on it, the median of the dilation angle is H/(L/2), where L/2 is the median of the positions of this irregularity on the joint lower wall. It is easily understood that the increase of heights of meaningful irregularity (and therefore of dilation angles) is much slower than the area increase. Therefore, this model (Fig. 20) favours the appearance of normal scale effects on dilation angle and on strength.

Experimental data is available for showing that mismatched joints have normal scale effects and matched joints present inverse scale effects (Kutter & Otto 1990) completely corroborating the considerations of this paper.

Therefore, the *in situ* observation of joint wall matching is the fundamental rule to program sliding tests. Only residual parameters must be taken into account if their mismatching overcomes the peak conditions and these residual parameters are little or not affected by scale effects. Peres Rodrigues & Charrua Graça's model must be used whenever peak conditions are not reached and when there are mismatchings. Actually, these authors demonstrate the excellent correlation between their model and Bandis' tests (1980) on mismatched samples exhibiting the so called "rocking" effect, considering that Bandis obtained normal scale effects. It is necessary to consider all dilation angles corresponding to several roughness and undulation orders and also of their amplitudes (which are not clearly taken into account by any known strength model) if the joints are matched. In these cases, Patton's model is usually used.

Even so, it may be observed in the field that shear displacements are clearer at joints as discontinuity sizes in-

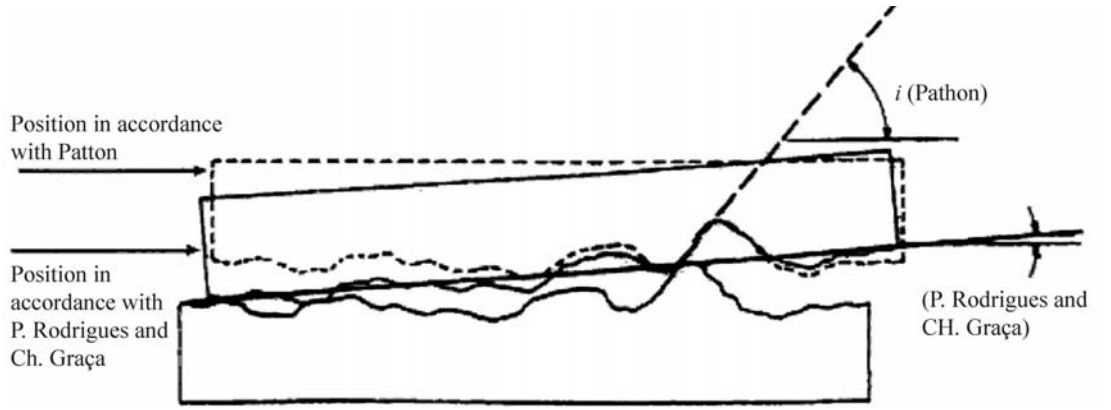

Figure 20 - Peres Rodrigues & Charrua Graça's sliding model (1985).

crease. It may be even asserted that shear displacements are always present in large crustal features. It is known that simple joints may have not only tensile origin but also shear or mixed origins and there are also frequently mismatched discontinuities. The situation is made worse by weathering and crushed zones.

Nevertheless, the problem is put on the unsafe side of engineering countless times because, despite the care in levelling the middle joint planes, the small samples from these mismatched joints are put into their best wall matching before the tests in sliding machines (the principle of adding the dilation angles applies here). If, for *in situ* tests, large samples are matched, inverse scale effects with small sample testing are obtained and the small samples will be on the safe side of engineering, but shear displacements are very probable for features having large areas, as the discontinuities are mismatched and that principle is not applicable. Thus, Peres Rodrigues & Charrua Graça's model is more adequate in such cases and so, normal scale effects correspond to these mismatched *in situ* conditions. Probably small sample tests, *in situ* tests and mainly, the conditions of discontinuities included in rock masses, are not comparable.

Therefore, the *in situ* observation of features matching is essential for the assessment of the significance of large and small tests. Mismatched roughnesses and undulations are partially inoperative for shear strength.

The results of Mac Mahon (1985) may only be understood within this scope, where he studied several joint slides by back analysis and found normal scale effects. He also concluded that small roughnesses had no influence in slides, with fillings and weatherings of those features probably only partially explain his results.

9. Conclusions

In spite of the obtained moderate correlation coefficients obtained in this experimental work, it allowed some essential rules to be highlighted. Many doubts about joint mechanical behaviour are solved by simple geometric considerations on the matter. Neglecting this principle may cause inadequacies in further rock joints test programs if some details of the testing execution are disregarded.

The interest of investigating the behaviour of small joint sample tests depends on the kind of scale effect that is sought, as they are on the safe side of engineering, if scale effects are inverse. Patton's model must be used if the rock mass joints are sound and matched. The advantage of the proposed test procedure, involving the levelling of joint middle planes, is to have demonstrated that small sample tests in dilation sliding phases are on the safe side of engineering. Mean amplitude and slope of roughness are reduced as sample sizes diminish, when joints are levelled. But mismatched samples obey Peres Rodrigues & Charrua Graça's model and the corresponding scale effects on strength are normal.

Many ideas and experimental regressions about joint mechanics must thus be reviewed because they do not fit the effects of a systematic levelling of sample middle planes on the roughness geometry in a dilating sliding phase.

Small samples may not be physically comparable with rock mass features from which they were withdrawn, depending on their dimensions, their matching or mismatching, the test techniques, their middle plane position, their weathering and crushed zones and on the sampled orders and levels of roughness and undulation.

Additionally, other important suggestions and conclusions applicable to matched and sound discontinuities, particularly if they have horizontal middle planes, were deduced from these tests. The following ones are pointed out:

Probably the maximum amplitude of roughness depends on the larger dimension of the joint and little or nothing on the smaller one. Samples having smaller linear dimensions have lower roughness amplitude and slope.

The anisotropy of roughness (anisotropies of direction and of orientation) increases as dimensions and plane symmetry of joint samples decrease. There is a general in-

crease of roughness symmetry and lower anisotropy as sample areas and their geometrical symmetry increase.

Average roughness increases as areas and dimensions of levelled samples increase (inverse scale effect).

The curvature of sliding trajectories has an obvious influence on the strength and on peak displacement. Longer mated samples have greater strength (and smaller peak displacement) when there are only the same undulation orders.

Sample strengths increase as the transverse dimensions to the sides (or widths) are reduced. The assessment of joint stability by the slices method is not appropriate because that effect puts them on the unsafe side of engineering. This effect worsens as σ_n, *JRC* and *JCS* increase. There is the possibility of the limit of this effect to be the REV of roughness anisotropy (Leal Gomes, 2002). More experimental work in this area is necessary to clarify this aspect.

As discontinuity scales increase (large joints, faults) the effect of previous shear displacements is clearer. Large active faults probably had overcame their peak conditions. Even so, they may have some dilation from their completely mismatched irregularities, which must be added to strength residual parameters in order to obtain their shear strength (Leal Gomes, 2001c).

The interest and significance of tests on small samples is very difficult to judge within the domain of mismatched joints. Therefore, there are situations where such tests are not advisable and, in these conditions, only the large *in situ* tests lead to reliable results.

References

Bandis, S. (1980) Experimental Studies of Scale Effects on Shear Strength and Deformation of Rock Joints. PhD Thesis, University of Leeds, 385 pp.

Bandis, S.C. (1990) Scale effects in the strength and deformability of rocks and rock joints. In: Scale Effects in Rock Masses, Loen, Balkema, Rotterdam, pp. 59-76.

Barton, N. (1990) Scale effects or sampling bias? In: Scale Effects in Rock Masses, Loen, Balkema, Rotterdam, pp. 31-55.

Barton, N. & Choubey V. (1977) The shear strength of rock joints in theory and practice. Rock Mechanics, v. 10, p. 1-54.

Brown, E.T. (1981) Rock Characterization, Testing & Monitoring - ISRM Suggested Methods. Pergamon Press, Oxford, 211 pp.

Charrua Graça, J.G. (1985) Heterogeneity and scale effect. Influence on the safety of rock mass works. LNEC, Lisbon, 137 pp. (in Portuguese).

Cunha, A.P. (1990) Scale effects in rock mechanics. Scale Effects in Rock Masses, Loen, Balkema, Rotterdam, pp. 3-27.

Gale, J.E. (1993) Fracture properties from laboratory and large scale field tests: evidence of scale effects. In: Scale Effects in Rock Masses, Lisbon, Balkema, Rotterdam, pp. 341-352.

Giani, G.P.; Ferrero, A.M.; Passarelo, G. & Reinaudo, L. (1992) Scale effect evaluation on natural discontinuity shear strength. In: Fractured and Jointed Rock Masses, Lake Tahoe, pp. 456-462.

Gracelli, G. (2001) Shear Strength of Rock Joints on Quantified Surface Description. PhD Thesis, École Polytechnique Federale de Lausanne, 126 pp.

Harrison, J.P. & Goodfellow, R.J.F. (1993) Effect of scale on roughness anisotropy and magnitude. In: Scale Effects in Rock Masses, Lisbon, Balkema, Rotterdam, pp. 111-117.

Hencher, S.R.; Toy J.P. & Lumsden A.C. (1993) Scale dependent shear strength of rock joints. In: Scale Effects in Rock Masses, Lisbon, Balkema, Rotterdam, pp. 233-240.

Kutter, H.K. & Otto, F. (1990) Influence of parallel and cross joints on shear behaviour of rock. In: Rock Joints, Balkema, Rotterdam, pp. 243-250.

Leal Gomes, M.J.A. (1998) O Efeito de Escala em Maciços Rochosos - O Caso da Resistência e Deformabilidade das Descontinuidades. PhD Thesis, University of Trás-os-Montes e Alto Douro, Vila Real, 303 pp. (The Scale Effect in Rock Masses - The Case of Joint Strength and Deformability).

Leal Gomes, M.J. (1999a) O Significado Prático dos Ensaios de Deslizamento de Descontinuidades em Maciços Rochosos. Geotecnia n. 87, p. 53-59 (The Practical Meaning of Shear Tests on Rock Mass Joints).

Leal Gomes, M.J.A. (1999b) A new approach to the scale effect on rock mass joint strength. 9th ISRM Congress, Paris, pp. 489-492.

Leal Gomes, M.J.A. (2000) The role of the amplitude of roughness on the shear strength of rock mass joints. EUROCK 2000 Symposium, Aachen, pp. 731-736.

Leal Gomes, M.J.A. (2001a) A general cause of scale effects in rock masses. 2001 ISRM Symposium - 2nd Asian Rock Mechanics Symposium, Beijing, Balkema, Rotterdam, pp. 613-618.

Leal Gomes, M.J.A. (2001b) The use of artificial joints executed in blocks of rock for the study of the mechanics of rock mass discontinuities. Ho & Li (eds), Geotechnical Engineering, Swets & Zeitlinger, Lisse, pp. 547-551.

Leal Gomes, M.J.A. (2001c) The assessment of safety of rock mass joints considering their amplitude of roughness. ISRM Regional Symposium EUROCK 2001, Espoo, Balkema, Lisse, pp. 249-254.

Leal Gomes M.J.A. (2002) The meaning of the perpendicular width to the joint sliding direction on the rock joint strength. ISRM India Symposium, New Delhi, pp. II-85-91.

Maerz, N.H. & Franklin, J.A. (1990) Roughness scale effects and fractal dimension. In: Scale Effects in Rock Masses, Loen, Balkema, Rotterdam, pp. 121-126.

Mc Mahon, B.K. (1985) Some practical considerations for the estimation of shear strength of joints and other discontinuities. Int. Symposium on Fundamentals of Rock Joints, Bjorklinden, pp. 475-485.

Muralha, J.J.R.D. (1995) Abordagem Probabilística do Comportamento Mecânico de Descontinuidades em Maciços Rochosos. PhD Thesis, Technical University of Lisbon, IST, Lisbon, 502 pp. (Probabilistic Approach of the Mechanical Behaviour of Rock Mass Joints).

Patton, F.D. (1966) Multiple Modes of Shear Failure in Rock and Related Materials. PhD Thesis, University of Illinois, 281 pp.

Peres Rodrigues, F. & Charrua Graça, J.G. (1985) Scale effect on the strength characteristics of rock masses. Proc. Int. Symp. on Role of Rock Mechanics in Excavations for Mining and Civil Engineering, Zacatecas, Mexico, pp. 405-408.

Pistone, R.S. (1990) Scale effect in the shear strength of rock joints. In: Scale Effects in Rock Masses, Loen, Balkema, Rotterdam, pp. 201-206.

Sage, J.D.; Aziz A.A. & Danek E.R. (1990) Aspects of scale effects on rock closure. In: Scale Effects in Rock Masses, Loen, Balkema, Rotterdam, pp. 175-181.

Swan, G. & Zongqi, S. (1985) Prediction of shear behaviour of joints using profiles. Rock Mechanics and Rock Engineering, v. 18, pp. 183-212.

Tse, R. & Cruden, D.M. (1979) Estimating joint roughness coefficients. Int. J. Rock Mech. Min. Sci. & Geomech. Abstr. v. 16, pp. 303-307.

Modeling the Influence of Biodegradation on Sanitary Landfill Settlements

Sandro Lemos Machado, Miriam de Fátima Carvalho, Orencio Monje Vilar

Abstract. This paper presents a mathematical model to reproduce long term or secondary settlement of sanitary landfills. Secondary compression is assumed to be commanded by two main processes: mechanical creep compression and the biodegradation of waste. The model introduces a biodegradation parameter that relates mass loss with volumetric variations. The biodegradation of Municipal Solid Waste (MSW) organic matter was represented through gas generation, modeled as a first order decay process. The gas generation was transformed into mass loss and used to evaluate biodegradation settlements through a mass balance equation. Some qualitative approaches concerning the time origin of secondary compression processes were addressed and used in the simulations. Strategies for obtaining model parameters are also presented and the main implications of biodegradation on settlement are discussed. The results predicted by the model are compared with laboratory and sanitary landfill data and reveal high levels of agreement between measured and calculated values.

Key words: municipal solid waste, mathematical model, settlement, creep, biodegradation.

1. Introduction

Sanitary landfill is the most commonly used method of final disposition of Municipal Solid Waste (MSW) around the world. These engineering structures pose a series of formidable challenges for geotechnical engineers as they have to deal with a complex material and address problems such as slope stability, stress on foundations and settlement.

Settlement in landfills is usually described as the result of primary and secondary compression. Secondary compression is usually attributed to mechanical creep of waste components and biodegradation. If a sanitary landfill is considered a biochemical reactor, as it usually is in Sanitary Engineering, the main inputs of this giant bioreactor are waste and water and the major outputs, gas and leachate. Landfill gas generation involves the depletion of organic waste and this process implies settlements that extend over many years until complete degradation of the organic matter.

Some of the mechanisms that control settlement are analogous to the settlement of soils and can be satisfactorily modeled through the theory of Soil Mechanics. However, the additional settlement generated by mass loss in the reactor is less well studied and this is a topic of concern among researchers studying of this issue. As gas generation is by far the most predominant output from the landfill, the quantification of gas generation rates and its equivalent loss of mass offers an attractive method to use to predict settlement. In this paper, a model to represent settlement in sanitary landfill caused by biodegradation is developed and tested against field settlement data. The model is intended to improve the constitutive model of MSW developed by Machado *et al.* (2002) as it incorporates a new approach to settlement in sanitary landfills.

2. Fundamentals

2.1. MSW compression

Although geotechnical engineers are used to dealing with natural materials that follow constitutive laws which are not completely understood, when dealing with MSW they face a heterogeneous material made up of different components, each with their own peculiar behavior. MSW is also subject to chemical and biological processes that alter its composition and mechanical behavior over time. These features in particular impart many peculiarities to landfill settlement making the entire process influenced by a multitude of mechanisms.

A qualitative model to represent the compression behavior of waste was presented by Grisolia & Napoleoni (1996), which is schematically shown in Fig. 1. A general description of the compression behavior of urban waste, which matches the indications in Fig. 1, was presented by Manassero *et al.* (1996) who described the compression behavior of urban waste as composed of the following mechanisms: I) physical compression, governed by mechanical distortion, bending, crushing and reorientation of waste components; II) raveling settlements due to migration of small particles into voids among large particles; III) viscous behavior and consolidation phenomena involving both solid skeleton and single particles or components; IV) decomposition settlement due to the biodegradation of the organic components and V) collapse of components due to physico-chemical changes such as corrosion, oxidation and degradation of inorganic components.

Sandro Lemos Machado, Associate Professor, DCTM, Universidade Federal da Bahia, Salvador, BA, Brazil. e-mail: smachado@ufba.br.
Miriam de Fátima Carvalho, Associate Professor, Escola de Engenharia, Universidade Católica do Salvador, Salvador, BA, Brazil. e-mail: miriam@ucsal.br.
Orencio Monje Vilar, Professor, Departamento de Geotecnia, EESC-USP, São Carlos, SP, Brazil. e-mail: orencio@sc.usp.br.
Submitted on June 2, 2008; Final Acceptance on November 5, 2008; Discussion open until April 30, 2009.

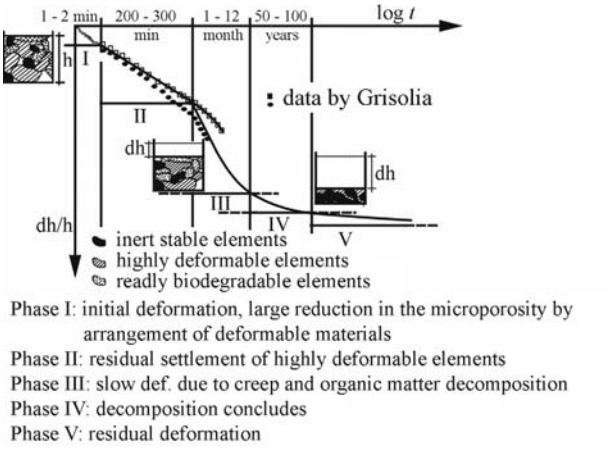

Phase I: initial deformation, large reduction in the microporosity by arrangement of deformable materials
Phase II: residual settlement of highly deformable elements
Phase III: slow def. due to creep and organic matter decomposition
Phase IV: decomposition concludes
Phase V: residual deformation

Figure 1 - Schematic view of the MSW compression process. Grisolia & Napoleoni (1996).

MSW settlement has been modeled taking into consideration that it is governed by primary and secondary compression and by using conceptual models similar to those developed for soils (Sowers, 1973; Yen & Scanlon, 1975; Edil *et al*., 1990; Bjarngard & Edgers, 1990; Edgers *et al*., 1992; Park & Lee, 1997; Ling *et al.*, 1998 and Gabr *et al.*, 2000).

Some attempts have been made to represent biodegradation. Edgers *et al.* (1992) associate settlement to waste degradation caused by bacteria growth and Soler *et al.*(1995) relate volume decrease to the generation of methane. McDougall & Pirah (2004) have described and proposed some phase relationship for decomposable soils that may also represent the biodegradation of organic matter in a landfill. They identified a relationship between void volume changes and decomposition of solid matter that depends on a single parameter, which they call decomposition-induced void change parameter. This parameter was shown to be indicative of mechanical consequences of decomposition and its use has provided a convenient reproduction of lab data of settlement of a decomposable soil.

Marques *et al.* (2003) have developed a composite rheological model and a computer program to predict landfill settlement. The composite model considers primary and secondary mechanical compression, as well as compression from biodegradation. In this model, the secondary biological compression due to the degradation of the material is based on the solution of Park & Lee (1997), which correlates the process of material loss through biological degradation and the associated secondary settlements to the solubilization rate of the degradable matter in the solid waste.

2.2. Gas generation and MSW loss of mass

Many factors interfere in the generation of gas in a landfill. The most important of these include waste composition and the presence of readily degradable organic components, the moisture content, the age of the waste, pH and temperature. The pH and temperature are relevant to the existence and action of bacteria. For instance, the optimum pH range for most anaerobic bacteria is close to neutral (McBean *et al.*, 1995).

Temperature conditions within a landfill influence the type of bacteria that predominate and the level of gas production. After initial relatively elevated temperatures, the temperature decreases within a landfill as anaerobic conditions develop. It has been recognized that optimum temperatures for methanogenic activity within a sanitary landfill range from 30 to 40 °C, and temperatures below 15 °C inhibit this activity (McBean *et al.*, 1995). The principal constituents present in landfill gas are methane (CH_4) and carbon dioxide (CO_2), but landfill gas is commonly saturated by water vapor and presents small quantities of non-methane organic components and various other trace compounds.

There are a variety of methods and models that can be used to estimate the methane and biogas generation rate at landfills (Ehrig, 1996; USEPA, 1996; USEPA, 1998). The USEPA (1998) landfill air emissions estimation model, represented by Eq. (1), however, is generally recognized as being the most widely used approach. It is a first-order decay model, recommended by the Intergovernmental Panel on Climate Change (IPCC, 1996) for calculating methane emissions from landfills. In this equation, Q = Methane generation rate (m^3/yr), L_o = Methane generation potential (m^3/Mg of waste), R = Landfill average annual waste acceptance rate (Mg/yr), k = Methane generation rate constant (1/yr), c = Time since to landfill closure (yr) and t = time since landfill opened (yr).

$$Q = L_0 R(e^{-kc} - e^{-kt}) \quad (1)$$

The value of k is affected by a large number of factors, such as waste composition, moisture content and disposal conditions. Values of k around 0.2 yr^{-1}, which correspond to a half life of about 3 years, are associated to elevated temperatures, high moisture contents and large amounts of food waste. Values of k around 0.03 yr^{-1} are associated with dry and cold environments in developed countries. According to USEPA (1998), L_o values vary between 6.2 and 270 m^3 CH_4/Mg of waste. Developing countries often present higher L_o values, although in humid tropical regions, the large moisture content decreases the amount of available dry mass by Mg of MSW.

Besides field measurements of gas production, the parameters k and L_o can be obtained using different approaches. IPCC (1996) presents equations that use the waste degradable organic carbon fraction, DOC, in order to estimate L_o. As DOC for some fractions has average known values, waste characterization data is sometimes used to obtain L_o. A more detailed discussion on this theme can be found in Bingemer & Crutzen (1987).

3. The Proposed Model

The influence of the biodegradation processes and resulting mass loss on the field settlement is initially assessed considering the phase diagram presented in Fig. 2. In this figure, v_a, v_w, v_s are the volumes of air, water, and solids respectively, and v is the total volume. m_w, m_s, and m are the corresponding mass of these phases. The assumptions of the model by Machado *et al.* (2002) are adopted in this paper and they consider that the mechanical behavior of waste is controlled by two different effects: a) the reinforcement of MSW by the fibers (mainly composed of many types of plastics) and b) the behavior of the MSW paste, that is all the other non fibrous materials. Therefore the MSW solids are divided into two: fibers and paste solids. Eqs. (2) and (3) express these assumptions mathematically and the additional subscripts, *f* and *p*, refer to fibers and paste respectively.

$$v_{sf} + v_{sp} = v_s \tag{2}$$

$$m_{sf} + m_{sp} = m_s \tag{3}$$

Additionally, fibers are considered as having no voids, *i.e.* all the MSW voids belong to the paste. This means that solid fibers volume (v_{sf}) is similar fibers volume (v_f), ($v_{sf} = v_f$) and that:

$$v_p = v_{sp} + v_v \tag{4}$$

Figure 3 sketches the volume variation associated to the biodegradation of MSW. The resultant MSW volume variation, Δv, is computed through α factor by:

$$\Delta v = (1+\alpha)\Delta v_s \tag{5}$$

The fiber components do not supposedly lose mass over time, thus the solid volume change considered before corresponds to the paste volume variation ($\Delta v_s = \Delta v_{sp}$). The Eqs. (6) and (7) express the effect of the loss of mass on MSW void ratio and volumetric strain. In these equations, *e* refers to the MSW void ratio. In these equations, the subscript *o* refers to initial condition and the subscript *d* that the variations are due to the biodegradation process.

$$\Delta e_d = \frac{v_{vo} + \alpha\Delta v_s}{v_{so} + \Delta v_s} - \frac{v_{vo}}{v_{so}} = \frac{\alpha - e_o}{\frac{v_{so}}{\Delta v_s} + 1} \tag{6}$$

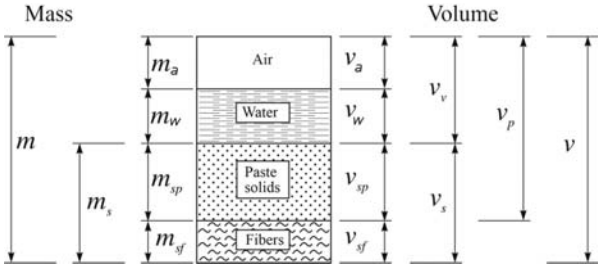

Figure 2 - MSW phase diagram.

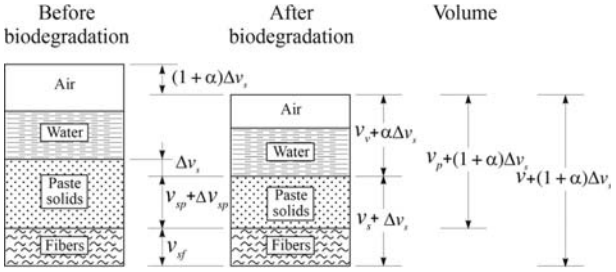

Figure 3 - Phase diagram illustrating the effect of the mass loss on the MSW volume.

$$\varepsilon_{vd} = \frac{-\Delta v}{v_o} = \frac{-\Delta v_s(1+\alpha)}{v_{so} + v_{vo}} = \frac{-\Delta v_s(1+\alpha)}{(1+e_o)v_{so}} \tag{7}$$

The α parameter, which is identical to that proposed by McDougall & Pirah (2004), expresses the fact that the additional volume variation associated with biodegradation will not produce equivalent waste compression, but rather some waste deformation that depends on the relative values of α and e_o. Furthermore, the voids generated by the decomposition process induce modifications in the waste structure which can lead to additional compression. As a first qualitative analysis it is worth commenting that if α is smaller than e_o, the MSW void ratio will increase (at least theoretically) leading to a looser waste, whereas α values larger than e_o tend to increase the waste dry density. In the particular case of α equal to e_o, biodegradation volumetric strain will arise but the relative void variations of paste and that of the waste keep the same void ratio. Finally, it should be emphasized that some tests and field results suggest that the α parameter is not a constant value, but a function of the MSW biodegradation stage and probably other variables, such as confining stress, waste composition, which will be discussed later.

Equations (6) and (7) can be rewritten, including the values of ρ_s and ρ_{sp} to calculate v_{so} and Δv_s if the initial MSW dry mass and the amount of loss of mass are known. This gives rise to the following equations:

$$\Delta e_d = \frac{(e_o - \alpha)}{\frac{m_{so}\rho_{sp}}{-\rho_{so}\int_o^t \frac{\partial m_s}{\partial t}\,dt} - 1} \tag{8}$$

and

$$\Delta\varepsilon_{vd} = \frac{-\rho_{so}\int_o^t \frac{\partial m_s}{\partial t}\,dt\,(1+\alpha)}{(1+e_o)m_{so}\rho_{sp}} \tag{9}$$

Equation (10) puts Eq. (9) in an incremental way.

$$d\varepsilon_{vd} = -\left(\frac{\rho_{so}}{\rho_{sp}}\right)\left(\frac{1}{1+e_o}\right)(1+\alpha)\frac{\partial m_s}{\partial t}\frac{1}{m_{so}}dt \qquad (10)$$

In Eqs. (8) to (10), ρ_s and ρ_{sp} are the specific densities of MSW solids and of paste particles respectively. ε_v refers to the MSW volumetric strain. The specific density of biodegradable paste solids was introduced to consider that the material to be decomposed differs in density from the inert material.

In many instances, the creep compression of MSW has been successfully modeled by the Gibson & Lo (1961) proposition. It is a simple model, requiring the use of only one variable. In this case, the MSW creep compression is:

$$d\varepsilon_{vc} = \frac{c_\alpha\, dt}{(1+e_o)\ln(10)\,t} \qquad (11)$$

In this equation, C_α = MSW secondary compression index and $d\varepsilon_{vc}$ = volumetric strain increment expected as a function of the MSW creep compression. As secondary compression is being considered as composed of mechanical creep compression and of biodegradation compression, it is now possible to calculate the increment in the MSW volumetric strain:

$$d\varepsilon_v = d\varepsilon_{vd} + d\varepsilon_{vc} = \left[\frac{c_\alpha}{(1+e_o)\ln(10)\,t} - \left(\frac{\rho_{so}}{\rho_{sp}}\right)\cdot \left(\frac{1}{1+e_o}\right)(1+\alpha)\frac{\partial m_s}{\partial t}\frac{1}{m_{so}}\right]dt \qquad (12)$$

The main hypothesis of this proposition rests on the fact that the MSW loss of mass can be calculated from gas generation data. This is made with the use of Eq. (13), where C_m is the organic matter methane yield, considering a complete methane conversion (m^3 CH_4/dry-Mg). The value of Q may be calculated using Eq. (1) if the first order decay method is used to predict the gas generation process.

$$-\frac{\partial m_s}{\partial t} = \frac{Q}{C_m} \qquad (13)$$

The use of Eqs. (1) and (13) conducts to Eqs. (14) and (15). Equation (14) is more appropriate for a global analysis, considering the landfill as a whole whereas Eq. (15) is more suited for numerical integration purposes.

$$-\frac{\partial m_s}{\partial t}\frac{1}{m_{so}} = \frac{L_o(1+w)(e^{-kc} - e^{-kt})}{C_m(t-c)} \qquad (14)$$

$$-\frac{\partial m_s}{\partial t}\frac{1}{m_{so}} = \frac{L_o k(1+w)e^{-kt}}{C_m} \qquad (15)$$

This way, Eqs. (12) and (15) (or Eq. (14)) encompass the complete formulation of the proposed approach in order to calculate MSW long term volumetric strains. It depends on the C_α and α parameters, together with the parameters related to gas generation which are L_o, k.

The coefficients of secondary compression, C_α and α, can be obtained from consolidation tests if enough time is allowed for mechanical secondary compression and mass loss to take place, or from back analysis of data from landfills. It is important to note that the time origin for creep compression and biodegradation may differ. It is usually assumed that creep compression starts immediately after waste landfilling and the start time can be roughly estimated from laboratory tests, analyzing the shape of the long term compression curves. The beginning of the biodegradation process is a much more complicated subject and is very difficult to estimate from laboratory tests as it is difficult to reproduce real field conditions. In places where favorable degrading conditions are present, biodegradation processes start very early. In this case, it is thought that the use of a common time origin for both processes, creep and biodegradation, is acceptable for practical purposes. In the absence of favorable conditions, there is a time delay in the biodegradation process that should be taken into account in the use of Eq. (12).

The parameters L_o and k can be obtained from the literature for certain conditions of waste composition, landfill operation and climate. L_o can also be obtained from laboratory tests designed to measure gas generation, such as BMP (Biochemical Methane Potential) tests. If BMP tests are performed using landfill samples of different ages, the k parameter can be derived. The other information needed includes the physical indexes of the waste, namely the initial void ratio and specific densities of paste, fibrous material and the MSW as a whole.

C_m values vary according to the waste component considered, but C_m values between 400 and 500 m^3 CH_4/dry-Mg are frequently found in published papers. According to Barlaz *et al.* (1990), values of C_m of 414.8 m^3 CH_4/dry-Mg and 424.2 m^3 CH_4/dry-Mg can be considered for cellulose and hemicellulose, respectively. Tchobanoglous *et al.* (1993) present biogas yields from 750 to 900 m^3/dry-Mg. As the biogas methane fraction usually varies from 0.5 to 0.6, similar values of C_m are predicted by the authors. If the waste composition is known, Eq. (16) (Tchobanoglous *et al.*, 1993) may be used to compute C_m values for different waste components and for the MSW as a whole. In Eq. (16), the indexes a, b, c and d are used to represent the empirical mole composition of the organic material. Table 1 shows waste components compositions (dry weight) suggested by Tchobanoglous *et al.* (1993) and Table 2 presents the values of C_m and water consumption predicted for each waste component.

$$C_aH_bO_cN_d + \frac{[4a-b-2c-3d]}{4}H_2O \rightarrow \frac{[4a+b-2c-3d]}{8}CH_4 + \frac{[4a-b+2c+3d]}{8}CO_2 + d\,NH_3 \qquad (16)$$

Perhaps the most difficult task is separating the contributions of parameters C_α and α, since this would require laboratory tests that extend over long time periods, and the α value is probably not a constant value throughout the decomposition process. Some possible ways to obtain these parameters are outlined below.

3.1. The nature and magnitude of the α parameter

Understanding the nature of the α parameter is a key task in accessing the influence of mass loss on MSW volumetric strains. The analysis of coupled laboratory or field data, where settlements and gas yields have been measured simultaneously can be used to determine α.

Mehta *et al.* (2002) describe a field experiment that was performed to evaluate the effects of leachate recirculation on waste decomposition and field settlement. The experiment comprised one control cell without any kind of treatment, and an enhanced cell that underwent leachate recirculation. Figure 4 presents data from Mehta *et al.* (2002), with respect to settlement and gas production in the control and enhanced cells analyzed.

Both cells initially had about 930 m^2 of surface area and were 12 m thick. Cells were filled from April through October 1995 and the final cover was put in place in November 1995. Settlement measurements and gas collection were initiated on 12 June 1996. After 1,231 days, cumulative methane production reached 63.1 and 27.9 m^3 CH_4/Mg of wet waste in enhanced and control cells, respectively. The corresponding average settlements were about 14.2% of the waste thickness in the enhanced cell and 2.74% in the control cell.

From the data presented by Mehta *et al.* (2002), the MSW initial densities were calculated and reached about 0.710 Mg/m^3 and 0.696 Mg/m^3 for the control and the enhanced cells respectively. The initial water content in both cells was assumed to be about 17.6% (average value, dry basis, obtained considering control cell samples).

In order to study the nature and magnitude of the α parameter gas generation data must be converted in loss of mass through C_m. Equation (17) was used to convert gas production in mass loss during a given time interval. In the absence of waste composition data a value of C_m = 450 m^3 CH_4/dry-Mg was employed.

$$-\frac{\Delta m_{s\,t_i}^{t_{i+1}}}{m_{so}} = \frac{\dfrac{\int_{t_i}^{t_{i+1}} Q\,dt}{m_o}(1+w)}{C_m} \tag{17}$$

Figure 5(a) presents the cumulated loss of mass calculated using Eq. (17) and data shown in Fig. 4(b). As it can be seen, enhanced cell presented a mass loss of about 17% while the loss of mass in the control cell was of about 7.4%. Data presented in Figs. 5(a) and 4(c) were used to study the influence of the loss of mass in the observed settlements along the decomposition process. Mass loss intervals

Table 1 - Waste components composition (% dry weight). Tchobanoglous *et al.* (1993).

Waste organic component	C	H	O	N	S	Ash
Food wastes	48.0	6.4	37.6	2.6	0.4	5.0
Paper	43.5	5.0	44.0	0.3	0.2	6.0
Cardboard	44.0	5.9	44.6	0.3	0.2	5.0
Textiles	55.0	6.6	31.2	4.6	0.2	2.5
Leather	60.0	8.0	11.6	10.0	0.4	10.0
Yard wastes	47.8	6.0	38.0	3.4	0.3	4.5
Wood	49.5	6.0	42.7	0.2	0.1	1.5

Table 2 - Organic matter methane yield (C_m) and water consumption according to Eq. (16).

Waste organic component	C_m (m^3 CH_4/dry-Mg)	H_2O consumption (H_2O kg/dry-kg)
Food wastes	505.01	0.26
Paper	418.51	0.20
Cardboard	438.70	0.16
Textiles	573.87	0.41
Leather	759.58	0.64
Yard wastes	481.72	0.28
Wood	484.94	0.24

$(-\Delta m_{s\,t_i}^{t_{i+1}} / m_{so})$ of about 5% were chosen and the induced settlement increments ($\Delta\varepsilon_v$) were computed to each cell. Figure 5(b) presents the obtained results in terms of the ratio $\Delta\varepsilon_v / [-\Delta m_{s\,t_i}^{t_{i+1}} / m_{so}]$. The results were plotted considering the average cumulated loss of mass of each interval.

According to data presented in Fig. 5(b), as the decomposition process goes on, the loss of mass becomes more effective in producing new settlements. This is particularly true if it is considered that the influence of the creep process tends to decrease along time. The behavior illustrated in Fig. 5 evidences that the α parameter is not constant along time, but tends to increase with the amount of organic matter already decomposed. Equation (18) was then used to calculate values of α to the same mass loss intervals employed in Fig. 5(b) and a linear relationship was adopted to fit the experimental results (Eq. (19)).

$$\alpha = \left[\Delta\varepsilon_v (1+e_o) - c_\alpha \log\left(\frac{t_{1+i}}{t_i}\right)\right] \cdot \left(\frac{\rho_{sp}}{\rho_{so}}\right) \frac{m_{so}}{-\Delta m_{s\,t_i}^{t_{i+1}}} - 1 \quad (18)$$

$$\alpha = \alpha_o + \alpha^* \frac{-\Delta m_s}{m_{so}} \quad (19)$$

where α_o refers to the initial value of α before any loss of mass, α^* refers to the rate of increase in the α values as the degradation process progresses and $-\Delta m_s/m_{so}$ corresponds to the cumulative loss of mass. According to McDougall & Pirah (2004), α must be equal or larger -1, as more negative values imply waste expansion as a consequence of mass loss, which seems not feasible physically. Values of α from -1 to 0 imply some degree of arching within the fill, in the sense that only a portion of the voids generated by the loss of mass will be compressed.

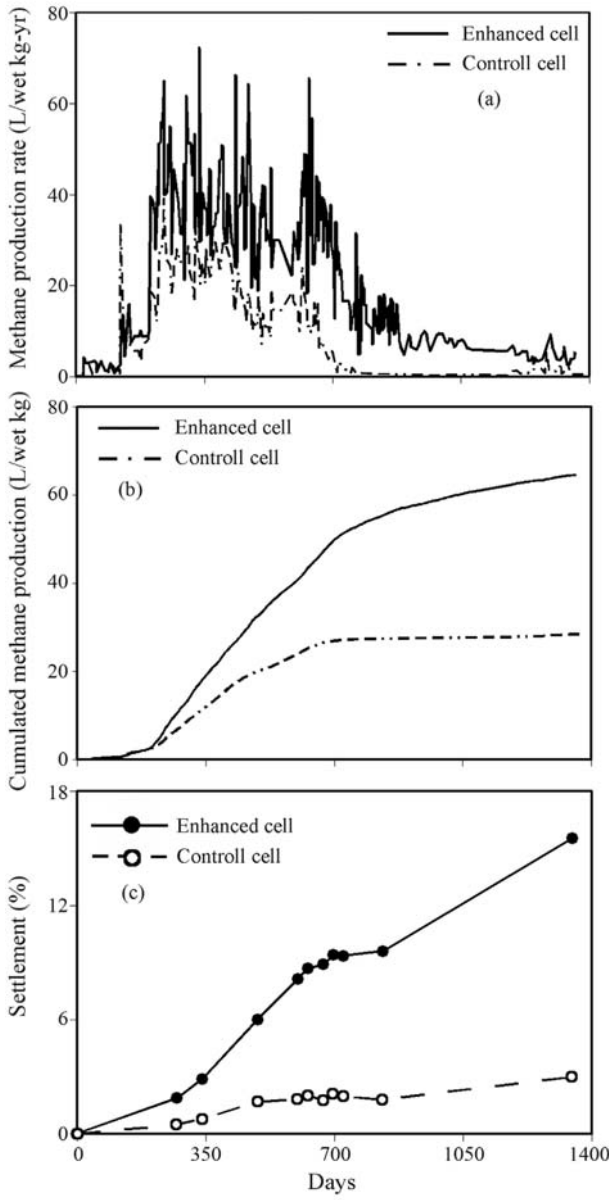

Figure 4 - (a) Methane production rate in enhanced and control cells, (b) cumulative methane production and (c) observed settlements. Metha *et al*. (2002).

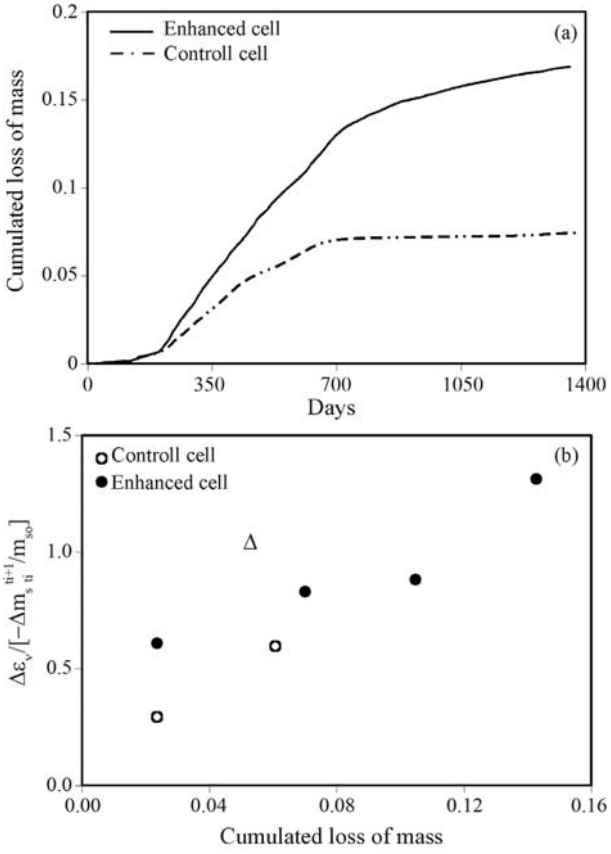

Figure 5 - (a) Cumulated loss of mass and (b) Influence of the loss of mass in the observed settlements.

The MSW particles specific density was assumed to be ρ_s = 1.75 Mg/m^3 and the paste specific density, ρ_{sp} = 1.8 Mg/m^3. These values were obtained from fresh waste from Salvador-Brazil (Machado & Carvalho, 2006). Initial void ratios of e_o = 1.90 and e_o = 1.96 were calculated for the control and enhanced cells, respectively. As the calculated values of α are C_α dependent, the value of C_α was chosen to produce α_o = -1 and then α_o = 0, when fitting Eq. (19) to experimental values. Values of C_α = 0.01, corresponding to α_o = 0 and α^* = 18.1 and C_α = 0.079, corresponding to α_o = -1 and α^* = 24.2 were found. Figure 6 shows the obtained results. As can be observed, the control cell presented smaller α values. The adjusted curves have the following coefficients of determination: r^2 = 0.87 for α_o = 0 and r^2 = 0.83 for α_o = -1.

The values showed above were used to calculate experimental settlements. Equation (20) was used for this purpose and Fig. 7 shows the obtained results. A value of $t_{o(creep)}$ = 255 days was adopted, corresponding to the period between the end of the filling process and the first settlement reading. The loss of mass that took place from the beginning of landfill to the first elevation measurement was ignored (this means that the time origin adopted for the mass loss process coincides with the beginning of the measurements: t_o = 0). This was considered a reasonable approach as the values of methane yields are quite small (Figs. 4a and 4b) at the beginning of the measurement process. As can be seen, the use of α_o = 0 yields calculated values that better fit the experimental data of both cells. It is believed that part of the observed scattering could be attributed to the fact that some variables such as the gas and settlement started to be measured just 8 and 17 months after the end of the filling process, respectively.

$$\varepsilon_v = \frac{(1+\alpha_o)\left[\frac{\int_{t_o}^{t} Q\,dt}{m_o}\right](1+w)\rho_{so}}{(1+e_o)\rho_{sp}C_m} + \frac{\alpha^*\left[\frac{\int_{t_o}^{t} Q\,dt}{m_o}\right]^2(1+w)\rho_{so}}{2(1+e_o)\rho_{sp}C_m^2} + \frac{C_\alpha \log\left(\frac{t}{t_{o\,(creep)}}\right)}{(1+e_o)} \quad (20)$$

Considering the results presented in Figs. 6 and 7 and the discussion presented before, it seems reasonable, for the sake of simplicity, to consider α_o = 0. It is believed that an eventual weakness of the model that could arise when assuming α_o = 0 can be counterbalanced by benefits of the use of only one variable, α^*. Assuming α_o = 0 implies that at the beginning of the biodegradation process, the mass loss increases the MSW void ratio. The resulting compression is equivalent to the voids left by the decomposed organic matter. The mass loss will increase the MSW void ratio until the value of $\Delta m_s/m_{so} = e_o/\alpha^*$ (at this moment, $\alpha = e_o$). From this moment on, additional mass loss will make the waste denser. The maximum value of α is limited by the maxi-

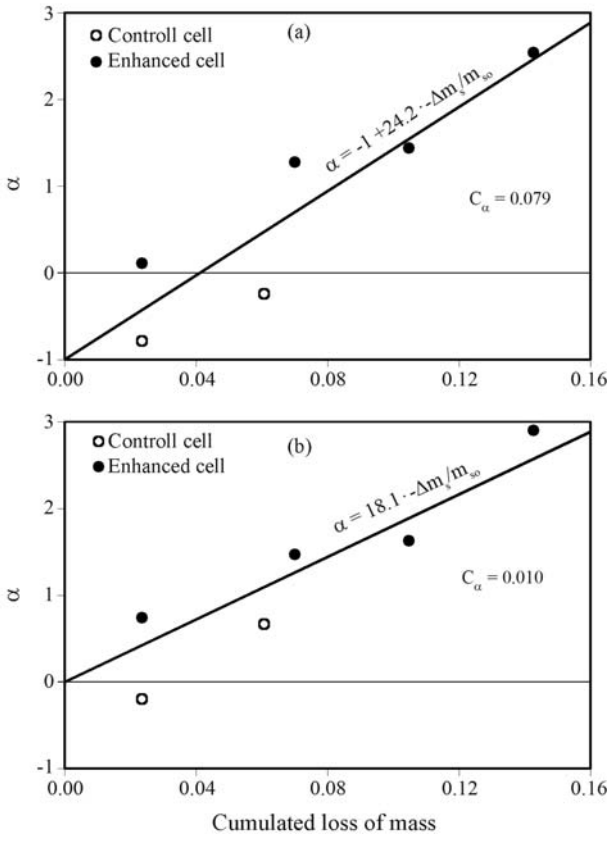

Figure 6 - Calculated values of α during the decomposition process. (a) C_α = 0.079 and α_o = -1 and (b) C_α = 0.01 and α_o = 0.

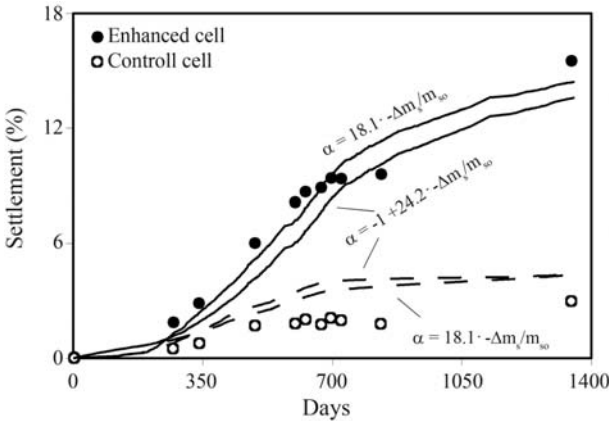

Figure 7 - Comparisons between measured and calculated values of settlements using the values of α_o and α* showed in the Fig. 6.

mum amount of organic matter available for decomposition, as expressed in Eq. (21).

$$\alpha_{max} = \alpha^* \frac{-\Delta m_{s(max)}}{m_{so}} = \frac{\alpha^* L_o (1+w)}{C_m} \quad (21)$$

If the enhanced cell is analyzed separately, a value of $C_\alpha = 0.041$ is needed to produce $\alpha_o = 0$ and a value of $\alpha^* = 17.8$ is obtained from best fitting. These parameters yield the calculated results shown in Fig. 8 that nicely match the experimental results. For numerical purposes, the incremental form of the equations to calculate long term variations in the MSW void ratio and volumetric strains are presented in Eqs. (22) and (23).

$$d\varepsilon_v = \left[\frac{c_\alpha}{(1+e_o)\ln(10)\,t} - \left(\frac{\rho_{so}}{\rho_{sp}}\right)\left(\frac{1}{1+e_o}\right) \times \left(1-\alpha^* \frac{\Delta m_s}{m_{so}}\right)\frac{\partial m_s}{\partial t}\frac{1}{m_{so}} \right] dt \quad (22)$$

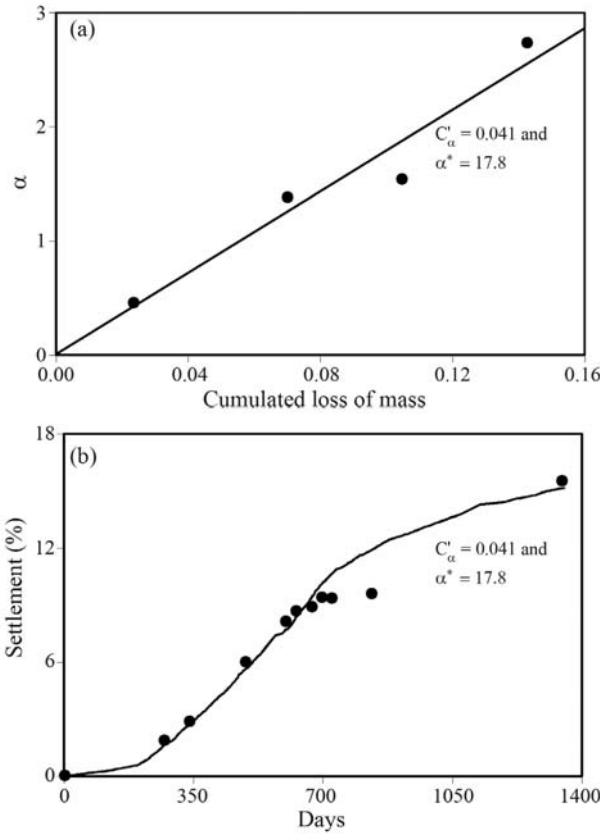

Figure 8 - (a) Calculated values of α during the decomposition process, adopting $C_\alpha = 0.041$ and $\alpha_o = 0$ in the enhanced cell. (b) Comparisons between measured and calculated values of settlements if only the enhanced cell is considered.

$$de = \left[\left(\frac{\rho_s}{\rho_{sp}}\right)\left(-\alpha^* \frac{\Delta m_s}{m_{so}} - e\right)\frac{\partial m_s}{\partial t} \frac{1}{m_{so}\left(1+\frac{\Delta m_s}{m_{so}}\right)} - \frac{c_\alpha}{\ln(10)\,t} \right] dt \quad (23)$$

3.2. Validation of the proposed model

Olivier & Gourc (2007) and Olivier *et al.* (2005) have presented other sets of data that allow to calculate the α parameter. The results refer to tests performed on a rigid cubic cell of about 1 m^3, in which MSW samples were tested under a vertical stress of 130 kPa. The enhanced tests, performed using leachate recirculation, presented coefficients of secondary compression, normalized through $(1+e_0)$, C^*_α, of about 0.32 during intense leachate recirculation and an average value of $C^*_\alpha = 0.072$. The standard or control test, without leachate recirculation, presented an average value of $C^*_\alpha = 0.035$, which is close to the C^*_α obtained in the enhanced test before the leachate recirculation phase, indicating the similar composition and behavior of the waste. The control test was performed during a period of 8.5 months whereas the enhanced test was performed during a period of about 22 months.

According to the framework presented in this paper, the differences observed in C^*_α values can be explained by the fact that in both cases this parameter embraces MSW mechanical creep and the secondary compression due to the mass loss. As the mass loss was more intensive in the enhanced tests, there was an increase in C^*_α values. The C^*_α values obtained by Olivier & Gourc (2007) can be related to the C_α and α^* values presented in this paper through Eq. (24).

$$c^*_\alpha = \frac{c_\alpha}{(1+e_o)} - \frac{\rho_{so}}{(1+e_o)\rho_{sp}\log\left(\frac{t}{t_o}\right)}\left(\frac{\Delta m_s}{m_{so}}\right) - \frac{\alpha^* \rho_{so}}{2(1+e_o)\rho_{sp}\log\left(\frac{t}{t_o}\right)}\left(\frac{\Delta m_s}{m_{so}}\right)^2 \quad (24)$$

The value of α^* can be obtained considering the difference between the measured C^*_α (see Eq. (25)) values in the control and enhanced tests. To apply Eq. (24) to both conditions, it was assumed that the decomposition process started just after two months from test beginning, in both cases. At this time, noticeable changes were observed in the CO_2 and CH_4 concentrations, indicating the beginning of anaerobic biodegradation. Considering the time period from this point up to the enhanced test final, an average value of $C^*_\alpha = 0.136$ is obtained. The values obtained for

log (t/t_o) were 1.05 and 0.63 considering the enhanced and control tests respectively. The MSW mass loss was about 17.9% in the enhanced tests and about 5.7% in the control. At the beginning of the secondary compression process, average MSW dry unit weight was about $\rho_d = 0.62$ Mg/m^3. Assuming $\rho_s = 1.75$ Mg/m^3 and $\rho_{sp} = 1.8$ Mg/m^3, it is possible to obtain $e_o = 1.82$. Using these values in Eq. (25), yields $\alpha^* = 16.7$.

$$c^*_{\alpha\,(enh)} - c^*_{\alpha\,(cont)} = \frac{\gamma_{so}}{(1+e_o)\gamma_{sp}}\left[\left(\frac{\frac{\Delta m_s}{m_{so}}\left\{1-\frac{\alpha^*}{2}\frac{\Delta m_s}{m_{so}}\right\}}{\log\left(\frac{t}{t_0}\right)}\right)_{enh} + \left(\frac{\frac{\Delta m_s}{m_{so}}\left\{1-\frac{\alpha^*}{2}\frac{\Delta m_s}{m_{so}}\right\}}{\log\left(\frac{t}{t_0}\right)}\right)_{std}\right] \quad (25)$$

According to Olivier *et al.* (2005) an average L_o reduction of about 40.9% in the BMP tests performed before and after the enhanced test was observed. Considering a period of 20 months of effective waste degradation and applying the first order decay method (Eq. (26)), a value of $k = 0.32$ yr^{-1} is obtained. As the intensity of the leachate recirculation varied during the test, the value of k obtained should be regarded as an average value. The relatively elevated value of k may be justified by the optimum controlled conditions of the test, which was performed with temperature control (≈ 35 °C) and leachate recirculation.

$$k = \frac{\ln\left(\frac{L_o(t)}{L_o(0)}\right)}{t} \quad (26)$$

The mass loss in the enhanced test can be calculated with the aid of Eq. (27). As before, t_o corresponds to the initial time assumed for the decomposition process (2 months) and t_f corresponds to the test duration (22 months). Eqs. (22) and (27) can now be used to predict the long term settlement obtained by Olivier & Gourc (2007). According to the authors, the secondary compression may be assumed as starting about 8 hrs after the test beginning. This was the initial time adopted for creep compression. The value of C_α was adopted as $C_\alpha = 0.035(1 + e_o)$, as the loss of mass was ignored at the test beginning (see Eq. (24)). Figure 9 presents the fit between the results calculated by the model and the experimental results obtained by Olivier & Gourc (2007).

$$\frac{\Delta m_s(t)}{m_{so}} = \frac{\frac{\Delta m_s(t_f)}{m_{so}}(1-e^{-k(t-t_o)})}{(1-e^{-k(t_f-t_o)})} \quad (27)$$

The framework developed here was also checked against field data from the Bandeirantes Landfill (Carvalho, 1999), located in the city of São Paulo, Brazil. Some data obtained from settlement plates installed there in conjunction with laboratory data (Vilar & Carvalho, 2004) using waste from the same landfill were used to test the ability of the model to reproduce field behavior.

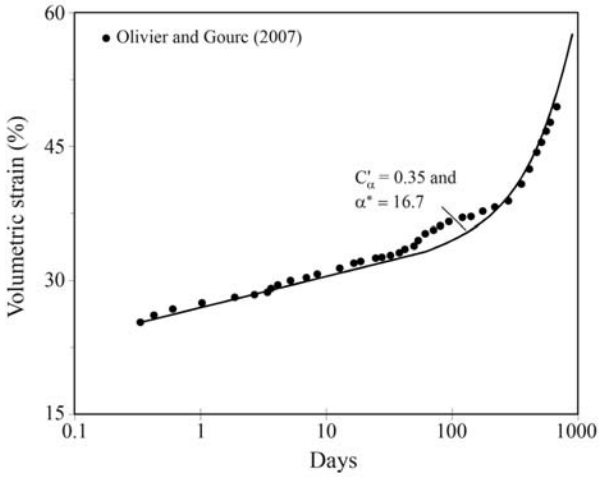

Figure 9 - Comparison between measured and calculated values of settlements. Experimental data obtained by Olivier & Gourc (2007).

Figure 10 presents data obtained from settlement markers SM 11, SM 12, SM1 3 and SM 21, located in the area AS2 of the Bandeirantes landfill. These markers correspond, respectively, to the following initial height of waste: 28 m; 37 m; 26 m and 58 m. The settlement data are supposed to represent only secondary compression, as the settlement markers were installed some months after the final cover. Although some differences can arise during filling at each location, just one simulation was carried out considering all measurement points, since the laboratory results were assumed to represent the average behavior of waste from all these places.

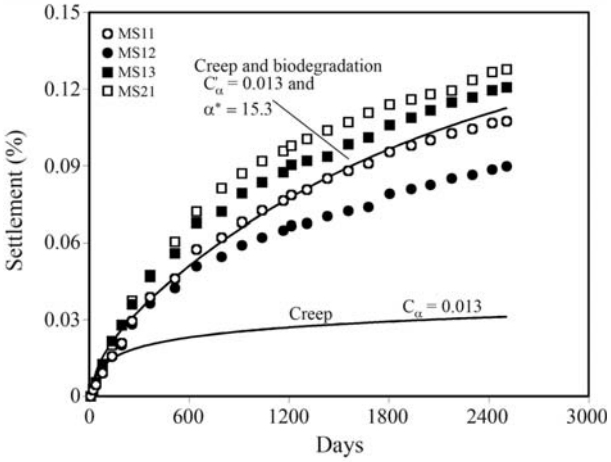

Figure 10 - Comparison between measured and calculated values of settlements from Bandeirantes landfill.

The landfilling of AS2 area started in January, 1981 and finished in October, 1991. Although the landfill procedures were not the same for all the locations in that area, these starting and closure dates were assumed to be the same for all the settlement plates. The first attempt to calculate field settlement data used Eq. (13), considering only mechanical creep compression, which was assumed as starting in October, 1991.

The comparison between calculated and field results is presented in Fig. 10. As can be seen, there is a good fit with the field results for the early stages of settlement. However, the model tends to underestimate the long term values, as one would expect. The tests carried out by Vilar & Carvalho (2004) lasted about 40 days and used 15 year old MSW. Therefore it is supposed that the effect of biodegradation is not incorporated in the obtained C_α and that this fact causes the model to underestimate the experimental field values.

A better adjustment is obtained when both mechanical and biodegradation creep is considered. These processes are embodied in Eq. (22). The following parameters were assumed considering the data presented by Britto (2006) when testing MSW from Salvador, Brazil: $k = 0.21$ year^{-1} and $L_o = 75$ m^3 CH_4/Mg of waste. An average α^* value of 15.3 was adopted, together with the values of ρ_s, ρ_{sp}, and C_m used in the previous simulation. The initial void ratio was estimated at 2.5 and this value is associated with an average water content of 50% and MSW initial density of $\rho = 0.75$ Mg/m^3. Equation (28) was used to compute the loss of mass from the beginning of the operation of the area AS2. In this equation, t_{op} refers to the operational time of the area before closure. The biodegradation process was taken as initiating just after waste filling as the long period of operation of area AS2 makes the influence of a time-lag in the calculated results negligible.

Figure 10 also includes the calculated values considering mechanical creep and biodegradation effects through Eq. (22). As can be seen, there is good agreement between field data and predicted values obtained for the settlement marker MS 11. The calculated values deviate slightly for the other points of measurement and the differences shown are believed to be due to the differences in landfilling procedures and on the assumption of parameters that rely on average values. It is believed that parameters resulting from tests specially designed to yield customized parameters or from back analysis of existing landfills, together with more precise construction data, such as times of beginning and closure of landfill, could improve model prediction as the general pattern of settlement curves are correctly duplicated by the model results.

$$\frac{\Delta m_s}{m_{so}} = \frac{L_o(1+w)\{(e^{k\,t_{op}} - 1)(e^{-k\,t_{op}} - e^{-k\,t}) + (k\,t_{op} - 1 + e^{-k\,t_{op}})\}}{t_{op}\,C_m\,k} \tag{28}$$

4. Conclusion

A comprehensive model to simulate secondary settlement of Municipal Solid Waste (MSW) has been developed and tested against real data from laboratory tests and landfills. Mechanical creep compression as well as biodegradation of waste were considered the main sources of secondary compression. Creep compression was modeled in a manner similar to that used for soils that exhibit creep considering that the process depends on a single parameter, the coefficient of secondary compression.

Phase relationships for degradable material are proposed and biodegradation volumetric variations are assessed through a single biodegradation parameter. The nature and magnitude of this parameter was analyzed considering some laboratory and field data available. It was shown that this parameter does not remain constant throughout the degradation process, but rather depends on certain variables. In the proposed model, it was assumed that the biodegradation parameter is dependent on the amount of organic matter already decomposed.

The depletion of organic matter in MSW was represented through gas generation, modeled as a first order decay process. The gas generated was transformed into mass loss and used to evaluate biodegradation settlement through a mass balance equation.

It was demonstrated that model parameters can be obtained from laboratory tests and from field data and certain strategies to relate biodegradation parameters to gas generation and the coupling of mass balance equation and settlement are presented. The model predictions provided data that compared favorably with laboratory and field data regarding settlement and thus imparted credibility to the model for predicting long term landfill settlements.

References

Barlaz, M.A.; Ham, R.K. & Schaefer, D.M. (1990) Methane production from municipal refuse: A review of enhancement techniques and microbial dynamics. Critical. Reviews in Environmental Control, v. 19:6, p. 557-584.

Bingemer, H.G. & P.J. Crutzen (1987) The production of methane from solid wastes. Journal of Geophysical Research, v. 92:2, p. 2181-2187.

Bjarngard, A. & Edgers, L. (1990) Settlement of municipal solid waste landfills. Proc. 13th Annual Madison Waste Conf., Madison, pp. 192-205.

Britto, M.L.C.P.S. (2006) Biogas Production Rate and MSW Biodegradation Parameters in the Metropolitan Center Landfill. Msc Thesis, Federal University of Bahia, Salvador, Brazil, 185 pp (in Portuguese).

Carvalho, M.F. (1999) Mechanical Behavior of Municipal Solid Waste. PhD Thesis, University of São Paulo, São Carlos, SP, Brazil, 300 pp (in Portuguese).

Edgers, L.; Noble, J.J. & Williams, E. (1992) A biologic model for long term settlement in landfills. Proc. Mediterranean Conf. on Environmental Geotechnology, Turkey, pp. 177 184.

Edil, T.B.; Ranguette, V.J. & Wuellner, W.W. (1990) Settlement of municipal refuse. Geotechnics of waste fills - Theory and practice, STP 1070. ASTM, pp. 225 239.

Ehrig, Hans-Jurgen (1996) Prediction of Gas Production from Laboratory-Scale Tests. Bergische Universitat Gesamthochschule Wuppertal Pauluskirschstr. 7, 42285 Wuppertal, Germany. Published in Landfilling of Waste; Biogas. Edited by Christensen, *et al.* E & F N Spon, London.

Gabr, M.A.; Hossain, M.S. & Barlaz, M.A. (2000) Solid waste settlement with leachate recirculation. Geotechnical News, Newsletter of the North American Geotechnical Community, v. 18:2, p. 50-55.

Gibson, R.E. & Lo, K.Y. (1961) A theory of soils exhibiting secondary compression. Acta Polytechnica Scandinavica, C10, 296, p. 1-15.

Grisolia & Napoleoni (1996) Geotechnical characterization of municipal solid waste: Choice of design parameters. Proc. 2nd International Congress on Environmental Geotechnics, Osaka, v. 2, pp. 641-646.

IPCC (1996) Revised 1996 IPCC Guidelines for National Greenhouse Gas Inventories: Reference Manual. Intergovernmental Panel on Climate Change.

Ling, H.I.; Leschchnsky, D.; Mohry, I. & Kawabata, T. (1998) Estimation of municipal solid waste landfill settlement. J. of Geotechnical and Geoenvironmental Engn., v. 124:1, p. 21-28.

Machado, S.L.; Carvalho, M.F. & Vilar, O.M. (2002) Constitutive model for municipal solid waste. J. of Geotechnical and Geoenvironmental Engn., v. 128:11, p. 940-951.

Machado, S.L. & Carvalho, M.F. (2006) Metropolitan center landfill-determination of the MSW specific density of solid particles. 7 pp. Internal report.

Manassero, M.; Van Impe, W.F. & Bouazza, A. (1996) Waste disposal and cointanment. Proc. 2nd Int. Congress on Environmental Geotechnics, Osaka, Japan, v. 3, p. 1425-1474.

Marques, A.C.M.; Filz, G. & Vilar, O.M. (2003) Composite compressibility model for municipal solid waste. J. of Geotechnical and Geoenvironmental Engn., v. 129:4, p. 372-378.

McBean, E.A; Rovers, F.A. & Farquhar, G.J. (1995) Solid Waste Landfill Engineering and Design. Prentice Hall PTR, Englewood Clifs, 521 pp.

McDougall, J.R. & Pyrah, I.C. (2004) Phase relations for decomposable soils. Geotechnique, v. 54:7, p. 487-493.

Mehta, R.; Barlaz, M.A.; Yazdani, R.; Augenstein, D.; Bryars, M. & Sinderson, L. (2002) Refuse decomposition in the presence and absence of leachate recirculation. Journal of Environmental Engineering, v. 128:3, p. 228-236.

Olivier, F. & Gourc, J.P. (2007) Hydro-mechanical behavior of municipal solid waste subject to leachate recirculation in a large-scale compression reactor cell. Waste Management, v. 27, p. 44-58.

Olivier, F.; Gourc, J.P.; Achour, F.; Morais, J. & Bayard R. (2005) Evolution of bio-physical and mechanical characteristics of MSW after 2 years incubation in a laboratory-scale bioreactor. Proc. 10th International Waste and Landfill Symposium, Sardinia 2005, Cagliari, Italy, CDROM.

Park, H.I. & Lee, S.R. (1997) Long-term settlement behavior of landfills with refuse decomposition. J. Solid Waste Tech. Manag., v. 24:4, p.159-165.

Soler, N.D.; Maher, A; Chae, Y.S. & Hamidi (1995) A conceptual model for transient settlements in waste fills. Proc. UNSAT'95, Paris, v. 1, pp. 411-416.

Sowers, G.F. (1973) Settlement of waste disposal fills. Proc. 8th Int. Conf. on Soil Mechanics and Foundation Engineering, Moscow, 2.2, pp. 207-210.

Tchobanoglous, G; Theisen, H. & Vigil, S. (1993) Integrated Solid Waste Management. McGraw-Hill, New York, 978 pp.

USEPA (1996) A Guide for Methane Mitigation Projects. EPA 430-B-96-081, 90 pp.

USEPA (1998) Landfill Air Emissions Estimation Model v. 2.01. EPA 68-D1- 0117, EPA 68-D3-0033, 94 pp.

Vilar, O.M. & Carvalho, M.F. (2004) Mechanical properties of municipal solid waste. Journal of Testing and Evaluation, v. 32:6, p. 438-449.

Yen, B.C. & Scalon, B. (1975) Sanitary landfill settlement rates. Journal of the Geotechnical Engineering Division, v. 101:5, GT5, p. 475-487.

List of Symbols

c: time since to landfill closure

C'_{α}: MSW secondary compression coefficient

C^{*}_{α}: MSW secondary compression index, involving creep and mass loss

C_m: methane specific yield

C_{α}: MSW secondary compression index

DOC: Degradable Organic Carbon fraction

dx: infinitesimal variation of x

dx_c: infinitesimal variation of x due creep process.

dx_d: infinitesimal variation of x due decomposition process.

e: MSW void ratio

k: methane generation rate constant

L_o: methane generation potential

m_{sf}, m_{sp}, m_w, m_s, and m: masses of fibers and paste solids, water, solids and total

MSW: municipal solid waste

Q: methane generation rate

R: landfill average annual waste acceptance rate

t: time since landfill opened, time elapsed

t_{op}: landfill operation time ($t_{op} = t - c$)

v_a, v_w, v_s, v_v, v_p and v: MSW volumes of air, water, solids, voids, paste and total

v_{sf} and v_{sp}: volumes of fibers and paste solids, respectively

w: MSW water content (dry basis)

x_o: initial value of variable x

α: parcel of MSW coupled long term compression generated by waste mass loss process.

A^*: rate of increment of the MSW coupled time differed compression

ρ_s: unit weight of the MSW components

ρ_{sf}: unit weight of the fiber components

ρ_{sp}: unit weight of the paste components

Δx: finite variation of the generic variable "x"

Δx_c: finite difference in variable x due creep process.

Δx_d: finite difference in variable x due decomposition process.

ε_v: MSW volumetric strain

Benzene Concentration in the Phases of Tropical Soils

Wisley Moreira Farias, Éder de Souza Martins, Eraldo Luporini Pastore,
Patrícia F. Lootens Machado, Inês Sabioni Resck

Abstract. This work evaluates tropical soil adsorption capacity of a hydrophobic compound (benzene). With such purpose, a lateritic soil poor in organic matter and a hydromorphic soil rich in kaolinite with a higher organic content were studied. The lateritic soil, rich in Al and Fe oxides, presented a higher sorption capacity in grain size terms for having a higher clay fraction which consequently favored a greater surface contact area, and in mineralogical terms for containing micro-aggregates of Al and Fe oxides, which may confine hydrophobic compounds. This study also compared the lateritic soil retardation factor with Batch Test sorption data. It is shown that the retardation factor for benzene may overestimate the concentration of the adsorbed phase, and thus underestimates the concentration in the effective dissolved phase. Also, a simplified model is presented to calculate benzene concentration in the various phases (free, dissolved and adsorbed) and in the pore-fluid of a lateritic soil in a saturated environment.

Key words: adsorption, benzene, retardation factor, model.

1. Introduction

Benzene is an important aromatic hydrocarbon present in various industrial petrochemical products, being petroleum and coal its main sources. In spite of its industrial importance, benzene is a compound which is highly toxic to human health, either through inhalation, contact with the skin or by ingestion, causing damages to the central nervous system and the possibility of cancer (Malansky & Malansky, 1997). Cairney *et al.* (2002) reported that human occupational activity exposed to volatile hydrocarbons in gasoline via excessive inhalation may produce cognitive or neurological effects.

Since benzene is one of the components of fuels, namely gasoline and diesel, in the event of accidents at gasoline stations, or during the transportation of these materials, serious environmental damage may be caused. This hydrocarbon is considered a volatile compound which is highly soluble in comparison with others compounds, such as benzene, toluene, ethylbenzene and xylenes (BTX), and may easily infiltrate the soil and reach water tables, seriously affecting the water quality (Ulrich, 1999). According to Corseuil & Fernandes (1999) the alcohol added to Brazilian gasoline favors co-solvency, increasing the solubility of BTX hydrocarbons.

The flow of volatile hydrocarbons contaminants such as benzene, through the preferential flow channels and pores in the soil is partitioned in free, water, volatile and adsorbed phases. This partition in adsorbed phases occurs through the adsorption of minerals and organic matter that comprise the soil. Each of these processes may occur in a higher or lower degree, depending on the physical and chemical characteristics of the soil, as well as a function of the contaminant volume and of the soil matrix geometry (Zytner, 2002, Farias, 2003, Fetter, 1993).

The flow mechanism, which generally orients chemical partition processes (dissolution and adsorption), is a slow diffusive flow, *i.e.*, less than or equal to 10^{-9} $m.s^{-1}$ (Rowe *et al.*, 1995, Donahue *et al.*, 1999).

The clay minerals and organic material in the soil (adsorbent) may adsorb hydrocarbons (adsorbate) weakly or strongly, depending on the intensity of interaction between adsorbent/adsorbate. Strong interaction indicates chemical adsorption or chemisorption, which are covalent bonds or electrostatic bonds between the molecule and the surface. This process may require high activation energy, which may be relatively slow and not very reversible. However, in physical adsorption the interaction is weak (as occurs with aromatic hydrocarbons such as benzene). The bonds are of low energy activation and the process is easily reverted. Sorption may occur at the liquid/solid or vapor/solid interfaces. The latter form of sorption also occurs with benzene, due to its high volatility (Shaw, 1975; McBride, 1994).

The *Batch Test* experiment evaluates absorption by estimating the partition coefficients between equilibrium solution, which is called adsorption coefficient or adsorption constant. The adsorption coefficient may be deter-

Wisley Moreira Farias, M.Sc., Departamento de Engenharia Civil e Ambiental, Faculdade de Tecnologia, Universidade de Brasília, Campus Universitário Darcy Ribeiro, Asa Norte, 70910-900 Brasília, DF, Brazil. e-mail: wisleymf@gmail.com.
Éder de Souza Martins, D.Sc., Centro de Pesquisa Agropecuária dos Cerrados, Empresa Brasileira de Pesquisa Agropecuária, Rod. Brasília/Fortaleza km 18, Pedologia Planaltina, 73301-970 Brasília, DF, Brazil. e-mail: eder@cpac.embrapa.br.
Eraldo Luporini Pastore, D.Sc., Departamento de Engenharia Civil e Ambiental, Faculdade de Tecnologia, Universidade de Brasília, Campus Universitário Darcy Ribeiro, Asa Norte, 70910-900 Brasília, DF, Brazil. e-mail: elpastore@uol.com.br.
Patrícia F. Lootens Machado, D.Sc., Instituto de Química, Universidade de Brasília, Campus Universitário Darcy Ribeiro, Asa Norte, 70904-970 Brasília, DF, Brazil. e-mail: plootens@unb.br.
Inês Sabioni Resck, D.Sc., Instituto de Química, Universidade de Brasília, Campus Universitário Darcy Ribeiro, Asa Norte, 70904-970 Brasília, DF, Brazil. e-mail: isresck@unb.br.
Submitted on Decmeber 10, 2007; Final Acceptance on November 7, 2008; Discussion open until April 30, 2009.

mined by the Freundlich isotherm, given by the following equation:

$$\frac{X}{M} = K_f C_e^{1/\omega} \quad (1)$$

where X = mass of the compound adsorbed by the soil (μg); M = mass of the adsorbent (g); K_f = equilibrium constant which indicates adsorption capacity ([μg.g]/[L.mg])$^{1/n}$; C_e = concentration of the equilibrium solution after adsorption (mg/L) and ω = constant indicating the intensity of sorption.

High 1/ω values indicate a greater affinity between absorbate and adsorbent. Thus, when ω is equal to 1, the equation of the isotherm describes a linear partition or partition between the two phases, called K_d. However, when 1/ω is different than 1, K_d becomes specific for the concentration in which is determined, and thus K_f becomes more adequate to describe the sorption.

The contribution of organic matter to sorption in the soil may be evaluated through the standardized adsorption coefficient for organic carbon content (K_{OC}). This may be calculated by the following relation for K_d or K_f:

$$K_f = K_{oc} f_{oc} \quad (2)$$

where f_{oc} (g.kg^{-1})is the mass of the fraction of organic carbon. The organic material (*OM*) mass percentage values may be converted to organic carbon content (*OC*), through the following expression:

$$K_{oc} = \frac{K_f \times 100}{MO\%} \times 1.724 \quad (3)$$

The conversion factor of 1.724 is produced by the average percentages of organic carbon of hummus composition, when the percentage of *OC* in the humus is 58%. However, some studies use a factor of 1.923, which corresponds to 52% of organic carbon (Kiehl, 1979).

Humus, which is developed organic matter, has a high molecular weight polydispersed in the soil matrix. Its composition rich in polymeric and aromatic compounds influences the wide superficial area of humus propitiating the adsorption of fulvic and humic acids. These compounds may also favor the adsorption of hydrophobic compounds (Chiou *et al*., 1983; Karickhoff *et al.*, 1979; Murphy *et al.*, 1994). The specific surface of the minerals and of the organic material may influence the adsorption process due to its area of contact. The specific surface area of the organic matter, the oxides of iron, gibbsite and kaolinite have the following respective values: 700, 400, 100 and 10 m^2.g^{-1} (Kiehl, 1979; Sposito, 1984).

Studies of the adsorption of hydrophobic compounds in soil profiles, conducted by Njoroge *et al*. (1998), presented decreasing results for K_d at depths, as a function of the nature and quantity modification in the organic matter of the profile. In deeper horizons hydrophilic organic compounds (fulvic and humic acids) decrease adsorption.

The retardation factor is one of the internationally used parameters in numeric models to determine the retention of contaminants in soil, being determined by the following equation (Rowe *et al*., 1995):

$$R = 1 + \frac{\rho K_d}{n} \quad (4)$$

where R is the retardation factor; ρ is the apparent dry density; K_d is the sorption coefficient; n is the total porosity.

This study aims to present a contribution towards understanding the adsorption process of hydrophobic compounds in tropical soils, using the Freundlich isotherm to determine the mass of soil contaminated by dissolved organic compounds. This provides data for the estimates of the adsorbed phase concentration which may be used in decision-making processes aimed at the remediation of soil contaminated by benzene. Furthermore, a simplified model is presented to estimate the partition of hydrophobic compounds in a saturated medium evaluated by a quantitative comparison and retardation factors.

2. Materials

Two samples of soil typical of the *Cerrado* (savanna) region in Brazil were selected. The first sample is a lateritic soil, of reddish color, collected from B horizon at a depth of 4 m. Its texture is silty clay, with a large quantity of granular structure and small pores. The other sample is a hydromorphic soil from A horizon collected at a depth between 0.5 and 10 cm. This superficial horizon is rich in organic matter, characterized by a black color, due to a sitly clay texture and a small quantity of aggregates with few roots. The two soils are visually homogeneous and isotropic. Table 1 presents geotechnical properties of the materials studied. The degree of flocculation is obtained by percentage difference between ultrasound and water-dispersible clay fractions. The degree of dispersion is obtained by percentage water-dispersible clay fraction.

3. Methods

The *Batch Test* was initiated with the preparation of a stock solution of 250,000 mg.L^{-1} of benzene diluted in methanol. Two grams of air-dried (2 mm) soil was weighed and placed in 5 amber glass flasks. Diluted benzene from the stock solution was added to each flask, all reaching a final volume of 10 mL. This test was conducted in triplicate. All the flasks were adequately sealed to retain benzene. Then, the samples were submitted to agitation with a shaker at a constant temperature of 23 °C for 4 h (Brusseau *et al*., 1991; Saison *et al*., 2004). This shake for 4 h instead 24 h was conducted to reduce microbiological benzene degradation.

After the agitation process, the samples were stored in refrigerators for 15 min for decantation. Five mL were re-

Table 1 - Soil Characterization (Farias, 2003).

Test	Lateritic	Gley A
Atterberg Limit		
Liquid limit-W_L (%)	41	46
Plastic limit-W_P (%)	29	35
Plastic Index-I_P (%)	12	12
Granulometry*		
Clay (%)	70	55
Silt (%)	25	30
Sand (%)	5	15
Degree of flocculation (%)	87.1	85.5
Degree of dispersion (%)	12.9	14.5
Chemical		
pH	5.70	5.20
Organic material (%)	0.41	5.44
Exchangeable cations ($cmol_c.cm^{-3}$)	6.4	159.8
Mineralogy		
Quartz (%)	30.2	42.2
Anatase (%)	1.57	0.93
Kaolinite (%)	24.6	41.4
Gibbsite (%)	25.5	4.6
Goethite(%)	4.6	2.2
Hematite (%)	7.5	0.0
Illite (%)	2.2	3.1
Vermiculite (%)	3.7	5.7
Hydraulic conductivity ($cm.s^{-1}$)	$3.7x10^{-7}$	$3.8x10^{-8}$
n (%)	55.9	65.0

*Grain size data obtained by ultra-sound waves using a laser beam grain size analyser.

moved for centrifugation, which was conducted at the Embrapa-Cerrados laboratory, in Brazil, with a refrigerated centrifuge at a temperature adjusted to 0 °C at 2000 rpm for 40 min. The suspension was collected for extraction of benzene in the aqueous phase equilibrium by a modification of the *US EPA* 1996 methodology, as described by Donahue *et al*. (1999). The benzene was extracted with the addition of 1 mL of the suspension of the posterior phase to a 5 mL bottle. Then, 3.3 mL of dichloromethane was added to extract the benzene. An internal standard of 0.2 mL of *p*-fluorotoluene at a concentration of 350 $mg.L^{-1}$ was determined. The material was then agitated for a few seconds for the complete extraction of the organic phase. A 2 μL portion was then removed for the quantitative analysis of the benzene in the solution, with an analytical curve as an internal standard, in a gas chromatograph equipped with a Varian Star 3400 C_X series flame ionization detector (CG/FID). Cleaning of the columns after the passage of each sample was done with the injection of 1 μL of dichloromethane.

3.1. The gaseous chromatography technique

A volume of 2 μL of extract of dichloromethane was injected in the "splitless" mode in a phase DB-5 (30 m x 0.25 mm x 0.25 μm) cast silicon capillary column under the following chromatographic conditions: the temperature of the injector was 220 °C; the temperature of the detector was 300 °C; the initial temperature of the method was 38 °C, at a heating rate of 5 °C/min, reaching a final temperature at 100 °C (5 min). The carrier gas used was N_2 5 mL/min and the H_2 pressure at the head of the column was 68.95 kPa. The quantification was performed using a benzene standard with 98% purity. The internal standard was added to the analytical curve in order to reduce injection and/or volume errors (Leite, 1998).

4. Results and Discussion

The benzene partition process to the solid phase, conducted through the *Batch Tests*, presented significant adsorption, as can be verified in Table 2. According to this data, the average percent adsorption values obtained for the lateritic and gley A soil were, respectively, 65.73% and 48.82%. The *Batch Test* assay also produced the standard deviations for the initial and equilibrium concentrations which are associated to the adsorption due to the inherent losses in this type of experiment and also because the adsorbent is highly volatile. Nevertheless, the results were satisfactory.

The adsorption isotherms may be verified in Figs. 1 and 2. The respective coefficient correlation values for the lateritic and gley A soils were respectively 0.8895 and 0.8731, which may be reported to the errors mentioned previously. The linear coefficient is greater for the lateritic soil, indicating greater initial adsorption.

Table 3 shows the data generated by the adsorption isotherms. The lateritic soil presented the highest adsorption coefficient, equal to 13.56 $mL.g^{-1}$, and consequently the highest degree of interaction between adsorbent and adsorbate (1/ω), equal to 0.774. However, based on the adsorption values observed in the literature, it may be stated that the adsorption values found are high for benzene in both soils. With regard to K_{oc}, a higher value for the lateritic soil was noted, mainly due to the low organic material content in relation to the gley A soil. This consistency regarding K_{oc} data in comparison with the literature may indicate that organic carbon does not directly control the sorption process of the soils studied.

The higher sorption (K_f) for the lateritic soil in comparison with the Gley A may be related to the physical and chemical characteristics of each soil. This may indicate that the grain size distribution of the former are comprised of 70% clay-sized particles, favoring a greater adsorbate/ad-

Table 2 - Basic *Batch Test* data.

Sample	C_o (μg/mL)[1]	C_e (μg/mL)	X (μg/mL)	ads (%)[2]	X/M (μg/g)
Lateritic	3.65 ± 0.49[3]	1.00 ± 0.3	2.65	72.60	13.25
	7.59 ± 0.31	1.85 ± 0.2	5.74	75.62	28.71
	11.17 ± 0.19	4.36 ± 7.1	6.81	61.00	34.06
	19.80 ± 0.30	9.41 ± 1.56	10.36	52.47	51.94
	53.41 ± 5.06	17.64 ± 1.03	35.77	66.97	178.83
Gley A	3.65 ± 0.49[3]	1.20 ± 0.13	2.45	67.23	12.27
	7.59 ± 0.31	3.66 ± 0.67	3.93	51.80	19.67
	11.17 ± 0.19	7.10 ± 0.28	4.06	36.39	20.32
	19.80 ± 0.30	9.30 ± 1.19	10.50	53.04	52.50
	53.41 ± 5.06	34.37 ± 0.80	19.04	35.65	95.20

[1]Initial concentration equal for both samples. [2]Percentage of absorbed benzene. [3]Standard deviation.

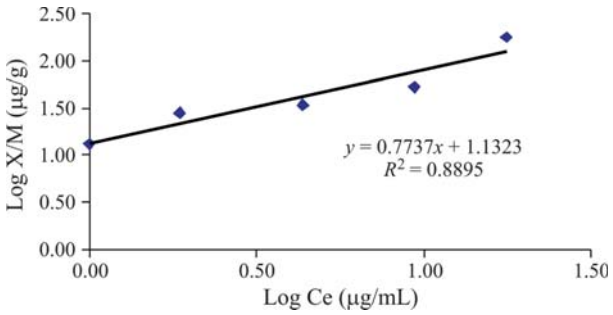

Figure 1 - Freundlich isotherm for the Lateritic soil.

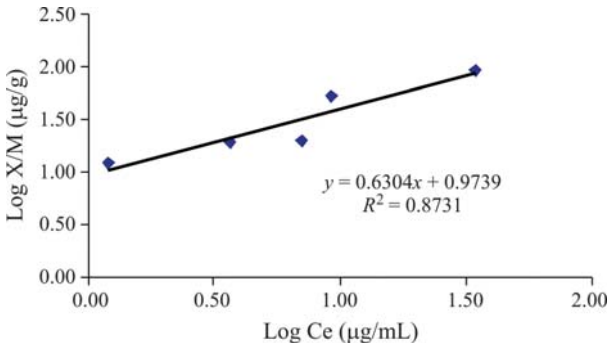

Figure 2 - Freundlich isotherm for the gley A soil.

sorbent interaction, due to the greater specific surface, which helps creating a larger contact area.

In mineralogical terms, the clay minerals of the lateritic soil contain a larger quantity of gibbsite and iron oxides. The Gley A soil contains a greater quantity of quartz, inert mineral, having few sites for the complex formation of minerals, organic matter, and hydrophobic compounds, which hampers the interaction between adsorbent and adsorbate. It also contains a larger quantity of kaolinite having a lower specific contact surface.

The type of organic material found in the lateritic soil (at a depth of 4 m), albeit low in quantity, may be largely comprised of fulvic and humic acids, which is different than the organic material found at the surface (humus), typical of the Gley A soil. This difference in organic material may influence the type of interaction between the organic mineral complex and the hydrophobic compound (Njoroge *et al.*, 1998).

Another factor to be considered regards the microaggregates and related soil micropores formed by the oxyhydroxides of Fe and Al. These may favor the confinement of non-adsorbed hydrophobic hydrocarbons in micropores. Thus, desorption data is superestimated because it included benzene in micropores.

The Gley A soil's exchangeable cations, although in greater quantities, given the higher organic matter content, did not prove to be an ideal parameter to verify adsorption

Table 3 - Freundlich isotherm data for the lateritic and Gley A soils in comparison with the literature.

Sample	K_f (mL/g)	1/ω	K_{co} (mL/g)	R^2	K_f (mL/g) literature*	K_{co} (mL/g) literature*
Lateritic	13.56	0.774	570.2	0.890	2.3-13.8[a]	83-2300[a]
					0.20-8[b]	-
Gley A	9.41	0.630	29.8	0.873	0.17-13[c]	26-59[c]

*Data of various soils. [a]Rowe *et al*. (1995). [b]Donahue *et al.* (1999). [c]Zytner (2002).

capacity. Figure 3 presents the benzene adsorption percentages, indicating the greater propensity of the lateritic soil in comparison with the gley A soil to adsorb (benzene) for the various concentrations observed.

4.1. Simplified model for the estimation of benzene concentration in a saturated soil

A scenario of 1 m^3 of homogeneous lateritic soil was proposed in order to estimate the concentration of Brazilian commercial gasoline, whose composition is 25% ethanol and 0.56% benzene. The soil characteristics were defined as follow: specific weight of 14.45 $kN.m^{-3}$, total porosity of 55.9%, degree of saturation (Sr) of 100%, and the soil's pores completely filled with water. In this situation, biological degradation factors which may influence the concentration of organic contaminants were not considered. In this regard, a leakage is assumed from a fuel tank containing 100 L of free phase of gasoline at the capillary edge interface with a saturated medium forming a Light Non-aqueous Liquid Phase (LNAPL). Thus, with gasoline having a density of 0.7663 $g.mL^{-1}$, there will be a mass of 429.1 g of benzene. The relevant properties of the gasoline were obtained from the National Petroleum Agency (ANP) laboratory in Brasília.

In order to compare the adsorption average from *Batch Test* with retardation factor it was considered 200.0 mg of benzene dissolved in the aqueous phase of 60% volume of water contained in a 1 m^3 soil volume. The benzene partition to the adsorbed phase under field conditions may take days to reach equilibrium due to the residual volume of benzene remaining trapped in the pores (Donahue, 1999). A difference was determined between the initial dissolved and adsorbed phases (FD_I) and the effective dissolved phase (D_E), or real free concentration. Based on the soil characteristics, the gasoline under study and data in the literature, the effective dissolved phase and the adsorbed phase were calculated. The effective dissolved phase was calculated with the retardation factor, and the adsorbed phase with the percentage of the dissolved phase extracted indirectly from arithmetic average of the adsorption percentages. Therefore, while the average adsorption of the lateritic soil was 66.0% the percentage of the effective dissolved phase was 34.3%. The results presented in Table 4 were obtained from these data.

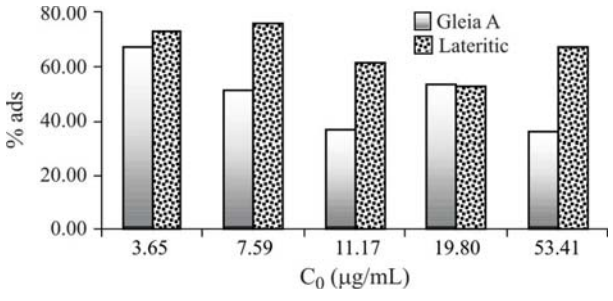

Figure 3 - Percentage of adsorbed benzene for the soils.

Table 4 - Calculations of the quantity of benzene partitioned in the soil and water.

FD_I (mg)	D_E (mg)	Adsorbed phase (mg)
200.0	5.55[a]	194.45[a]
200.0	68.54[b]	131.46[b]

[a]Calculation with the retardation factor. [b]Calculation with the average percentage obtained from the *Batch Tests*.

It may be seen in Table 4 that, from the result of the effective dissolved phase calculated by the retardation factor, it was possible to determine the adsorbed phase from the difference between FD_I and DE. Further analysis of the value obtained for the adsorbed phase indicates that it is overestimated, considering that maximum sorption in extreme conditions is empirically obtained by the *Batch Test*. However, maximum sorption would be 131.46 mg, which corresponds approximately to an average sorption of 66.0% in the *Batch Test*. From this perspective, the effective dissolved phase is underestimated when calculated by the retardation factor.

In order to calculate the concentration in the fluid-pore it is necessary to begin with the equivalent concentration for the soil, considering a contaminant mass in the initial dissolved phase (200.0 mg) in a given soil volume, which is expressed by the following equation:

$$C_E = \frac{M_{fd}}{V\rho} \tag{5}$$

where C_E = equivalent concentration (µg/g); M_{fd} = mass of the contaminant in the environment (mg); V = volume of the contaminated soil (m^3); ρ = density of the soil (kg/m^3).

Lastly, for the pore-fluid concentration the following equation is used:

$$C_p = \frac{C_E}{\frac{\theta_w}{\rho_w} + K_d} \tag{6}$$

where C_P = concentration of the pore-fluid ($\mu g.mL^{-1}$); θ_w = volumetric water content; ρ_w = water density ($g.mL^{-1}$); K_d = partition or adsorption coefficient ($mL.g^{-1}$).

The concentration in the pore-fluid is estimated at 0.010 $\mu g.mL^{-1}$ for K_d of 13.56 $mL.g^{-1}$ and the water density equal to 1 $g.mL^{-1}$. These estimates, besides being applications of the Freundlich isotherms, are important to support rapid decision making in the event of an accident involving contamination by hydrocarbons. The concentration in the pore-fluid may also be important for diffusive flow studies, or to better understand a non-saturated medium where the water content is lower or scarce.

5. Conclusions

The adsorption isotherms for both soils studied presented higher results in comparison with data in the literature. However, for the two soils studied, the one presenting the best result was the lateritic soil. This result differs from other studies that demonstrate greater sorption as a function of the high organic matter content. Nevertheless, the greater sorption may be related to the type of interaction formed among the mineral, the type of organic matter and the adsorbate. The texture of the soil may be one of the factors influencing adsorption in clay rich soils by favoring a greater interaction with adsorbate as a function of the greater specific surface. Another important aspect to be considered is the role of the micro-aggregates of Fe and Al oxides, which may confine the particles of adsorbate. In this study, a larger quantity of exchangeable cations did not influence sorption, although this was expected due to the absence of interaction between polar elements and hydrophobic compounds. Despite soil gley A having a larger specific surface, due to the larger amount of organic matter, its results for benzene adsorption were smaller than those of the lateritic soil. However, the adsorption process was greater in lateritic soil, probably because the influence of Fe and Al oxides micro-aggregates.

From the simplified model developed to estimate the concentrations of benzene partitioned in the various phases, it was observed that the retardation factor may overestimate the concentration in the adsorbed phase.

References

Brusseau, M.L.; Jessup, R.E. & Rao, P.S.C. (1991) Nonequilibrium sorption of organic chemicals: Elucidation of rate limiting processes. Environ. Sci. Technol., v. 25:1, p. 134-142.

Cairney, S.; Maruff, P.; Chis, B. & Currie, B. (2002) The neurobehavioural consequences of petrol (gasoline) sniffing. Neuroscience and Biobehavioral Reviews, v. 26:1, p. 81-89.

Chiou, C.T.; Porter, P.E. & Schmedding, D.W. (1983) Partition equilibrium of nonionic organic compounds between soil organic matter and water. Environ. Sci. Technol., v. 17:4, p. 227-231.

Corseuil, H.X. & Fernandes, M. (1999) Efeito do etanol no aumento da solubilidade de compostos aromáticos presentes na gasolina brasileira. Revista Engenharia sanitária e Ambiental, v. 4:1-2, p. 71-75. (Ethanol effect on the increasing in solubility of aromatic compounds present in Brazilian gasoline).

Donahue, R.B.; Borbour, S.L. & Headley. J.V. (1999) Diffusion and adsorption of benzene in Regina clay. Canadian Geotechinal Journal, v. 36:3, p. 430-442.

Farias, W.M. (2003) Condutividade Hidráulica de Solos Tropicais Compactados a Hidrocarbonetos da Gasolina. Dissertação de Mestrado, Departamento de Engenharia Civil e Ambiental, Universidade de Brasília, Brasília, 152 pp (Hydraulic conductivity of gasoline hydrocarbons in Tropical Compacted Soil).

Fetter, C.W. (1993) Contaminant Hiydrogeology. Prentice-Hall, New Jersey, 458 pp.

Karickhoff, S.W.; Brown D.S. & Scott, T.A. (1979) Sorption of hydrophobic polluatants on natural sediments. Water Research, v. 13, p. 241-248.

Kiehl, E.J. (1979) Manual de Edafologia: Relações Solo-Planta. Agronômica Ceres, São Paulo, SP, 262 pp (Edaphology Manual: Soil-Plant Relationships).

Maslansky, S.P.& Maslansky, C.J., Reinhold V. N. (1997) Health and Safety at Hazardous Waste Site. An Investigator's and Remediator's Guide to Hazwoper, New York, 612 pp.

McBride, M.B. (1994) Environmental Chemistry of Soils. Oxford University Press, New York, 406 pp.

Murphy, E.M.; Zachara, J.M.; Smith, S.C.; Phillips, J.L. & Weitsma, T.W. (1994) Interaction of hydrophobic organic compounds with mineral-bound humic substances. Environ. Sci. Technol., v. 28:7, p. 1291-1299.

Njoroge, B.N.K.; Ball,W.P. & Cherry, R.S. (1998) Sorption of 1,2,4-trichlorobenzene and tetrachloroethene within an authigenic soil profile: Changes in Koc with soil depth. Journal of Contaminant Hydrology, v. 29, p. 347-377.

Rowe, R.K.; Quigley, R.M. & Booker, J.R. (1995) Clay Barrier Systems for Waste Disposal Facilities. E & FN Spon, London, 390 pp.

Saison, C.; Perrin-Garnier, C.; Amellal, S.; Morel, J-L. & Schiavon, M. (2004) Effect of metals on the adsorption and extractability of 14C-phenanthrene in soils. Chemosphere, v. 55:3, p. 477-485.

Shaw, D.J. (1975) Introdução à química dos colóides e de superfícies. Edgard Blücher, São Paulo, SP, 185 pp (Introduction to Colloids and Surface Chemistry.).

Sposito, Garrison (1984) Surface Chemistry of the Soils. Oxford Univ. Press, New York, 234 pp.

Ulrich, G. (1999) The Fate and Transport of Ethanol-Blended Gasoline in the Environment. Governors' Ethanol Coalition, Lincoln, 88 pp.

US EPA (1986) Test methods for evaluating solid waste. Method 8020 A. In laboratory manual physical/chemical methods: v. 1B. United States Environmental Protection Agency, Washington, D.C. pp. 1-14.

Zytner R.G. (2002) Organic Compounds in Unsaturated Soil. ENGG 6670, Fall 2002 Soil overview_03.wpd. Available at www.soe.uoguelph.ca/webfiles/rzytner/HazWaste/soil_overview_03.pdf. Access in Abril 22, 2007.

Case History

Soils and Rocks
v. 32, n. 3

Grouting of TBM Rock Tunnel for the Pinalito Hydroelectric Plant, Dominican Republic

Marcos Eduardo Hartwig

Abstract. The Pinalito main hydroelectric tunnel, with a length of 11 km, is located in Cordillera Central mountain range, Dominican Republic. This mountain tunnel has been mined through extremely fractured andesitic-basaltic and rhyolitic tuffs. These rocks are been subjected to shear and collisional displacements between Caribbean and North America plates since middle Eocene. As a result, geological and hydrogeological conditions along the tunnel alignment are rather complicated. This paper presents the main aspects and results employed in order to overcome an unexpected water bearing incompetent rock zone, approximately eleven meters wide, that cross the tunnel alignment at Sta. 5+237.40. Ground treatment was well succeeded and took six months to be concluded. Procedures adopted took into account three steps, respectively: (1) geological drilling; (2) drainage; and (3) spilling and grouting injections.

Key words: grouting, Pinalito Hydroelectric Tunnel, TBM, water bearing incompetent rock zone, Dominican Republic.

1. Introduction

The Pinalito main hydroelectric tunnel, nearly 11 km in length, link the Dam to the Power House. It is located in Cordillera Central mountain range, eastern Hispaniola, which is divided between the countries of the Dominican Republic and Haiti. This mountain tunnel has been mined with a Robbins Open TBM (*Tunnel Boring Machine*), 3.66 m of diameter, through extremely fractured andesitic-basaltic and rhyolitic tuffs (Fig. 1).

The Hispaniola Island is located on the strike-slip suture line between Caribbean and North America Plate. Due the complex orogenic processes, multiple brittle tectonic structures affected the Cordillera Central mountain range, which resulted in a very complicated and highly variable geological, structural and hydrogeological ground condition.

Due to the lack of geological investigation, probe drilling and under evaluation of previously mined fault zones along the Pinalito main hydroelectric tunnel, an unexpected water bearing incompetent rock zone was reached at Sta. 5+237.40 and caused the TBM entrapment for six months. This paper presents the main aspects and results of treatment of the rock mass employed at Sta. 5+237.40, in the Pinalito main hydroelectric tunnel, Dominican Republic.

2. Tectonic Settings

The Hispaniola Island is located in the north edge of the Caribbean tectonic plate, which since middle Eocene is displacing to east in relation to the American tectonic plates (Fig. 2). This limit represents a complex deformation zone, in which is recorded collisional and left-handed strike-slip displacements. The Hispaniola Island consists of a terrain agglomeration, bounded by main fault zones, consolidated between lower Cretaceous and Miocene. Much of these limits were reactivated and form morphotectonic provinces made of narrow and elongated mountain ranges and sedimentary basins limited by faults (Fig. 3, Dolan *et al.* 1998, DeMets *et al.* 2000, Mann *et al.* 1991, Mann *et al.* 2002).

The Cordillera Central mountain range with summits over 3.000 m a.s.l. and WNW-ESE-trending, represents a cretaceous magmatic arc composed mainly of volcano-sedimentary and igneous rocks with occasional intercalations of cretaceous sedimentary rocks, slightly metamorphosed (Bowin 1966, Mann *et al.* 1991). The Pinalito main hydroelectric tunnel has been mined through extremely fractured bedded to massif andesitic-basaltic and rhyolitic tuffs, with maximum coverage thickness up to 550 m.

3. Geotechnical Aspects

The rock mass geotechnical classification adopted in the Pinalito main hydroelectric tunnel was the Q index (Table 1, Barton *et al.* 1974). Most of the tunnel mined before the fault zone at Sta. 5+237.40 was in rock class III to IV/V, which means, regular to poor rock mechanic quality (Fig. 4).

Immediately before the fault zone at Sta. 5+237.40, any anomalous geotechnical feature was detected, with exception of somewhat increase in groundwater infiltration.

4. General TBM Specifications

The Pinalito main hydroelectric tunnel has been mined by a Robbins open TBM built in 1981 and refurbished in 1983. It has 3.66 m of diameter and contains four electrical motors with 300 horse power each of it (Fig. 5A). The machine was not designed to operate through terrains with high groundwater flow, and does not present any pretreatment capabilities inside, such as probe drilling and

Marcos Eduardo Hartwig, M.Sc., Projetos e Consultorias de Engenharia LTDA. (PCE), Av. Presidente Wilson 165, Centro, Rio de Janeiro, RJ, Brazil. e-mail: marcoshartwig@yahoo.com.br.

Submitted on April 17, 2008; Final Acceptance on November 11, 2008; Discussion open until April 30, 2009.

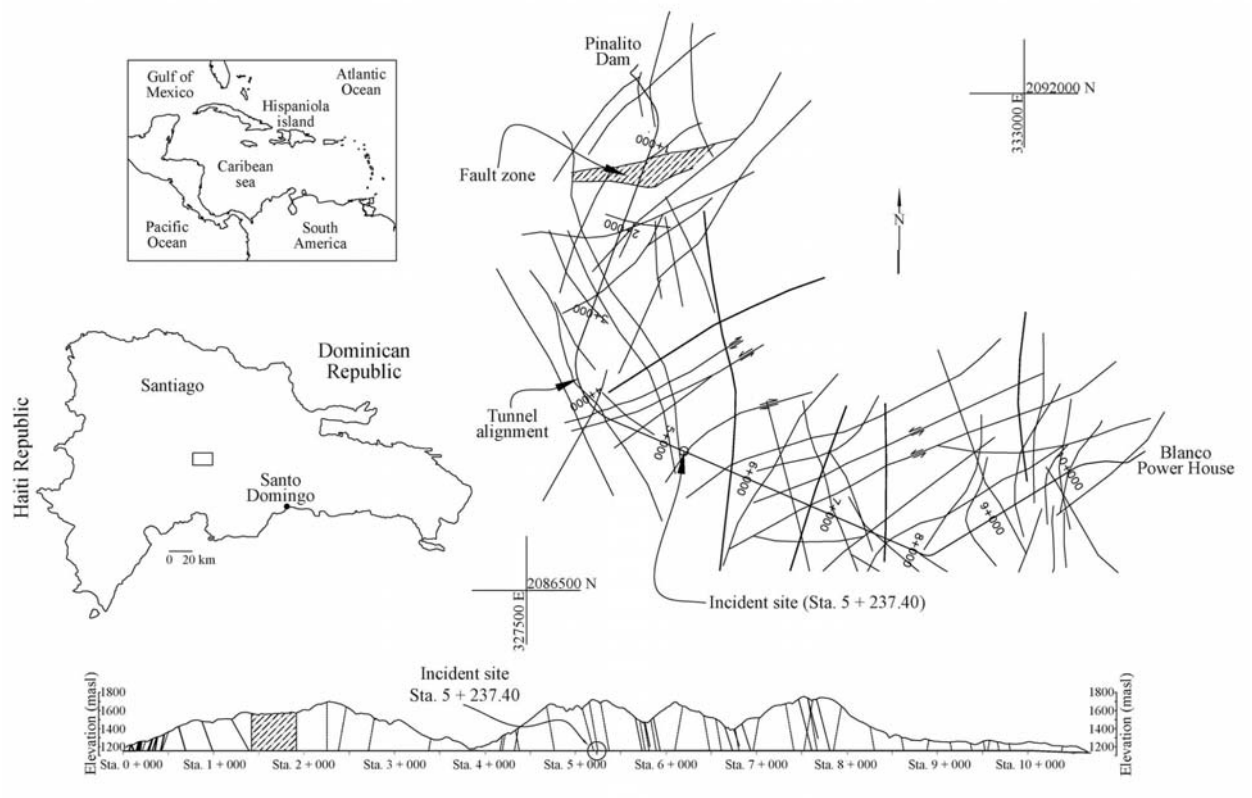

Figure 1 - Location of the Pinalito main hydroelectric tunnel. Geological profile and lineament map based on aerial photograph interpretation (scale 1:10.000) and field survey. Tunnel passes through cretaceous andesitic-basaltic and rhyolitic tuffs. UTM coordinate system, Zone 19Q, North Hemisphere.

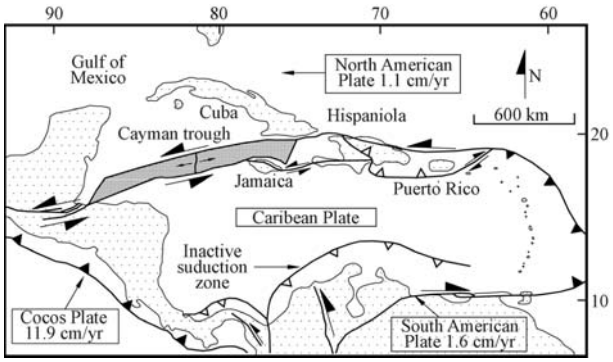

Figure 2 - Present-day plate structure of the Caribbean region. The island of Hispaniola straddles the active left-lateral strike-slip zone separating the North America and Caribbean plates. After Mann *et al.* (1991).

geophysics. For this reason, it was adapted an external rock drilling as showed in Fig. 5B.

5. Description of the Incident

Due to a combination of circumstances, such as lack of detailed geological investigation (overoptimism of geological underground conditions), probe drilling (related to operational difficulties) and production rates (and under evaluation of previously mined fault zone at Sta. 1+579 - due to its low water content), on march 26 of 2007, the excavation of the Pinalito main hydroelectric tunnel had to be stopped at Sta. 5+237.40, as it reached an unexpected water bearing incompetent rock zone, nearly eleven meters wide, which caused an extremely high pressurized groundwater influx into the tunnel (up to 460 L/s), followed by a rock collapse of the roof and face area over the TBM head.

6. Treatment Procedures

In order to overcome the extremely high groundwater influx into the tunnel related to this wide incompetent zone, three main steps were adopted, respectively: (1) geological drilling; (2) drainage; and (3) spilling and grouting injections.

6.1. Geological drilling

Horizontal geological drills were performed in order to investigate characteristics of the incompetent zone, like extent, direction and material contents. Basically it showed up a heterogeneous irregular-shaped incompetent zone of nearly N-S trending, with approximately eleven meters wide (Fig. 6). This zone cross the tunnel alignment at Sta.

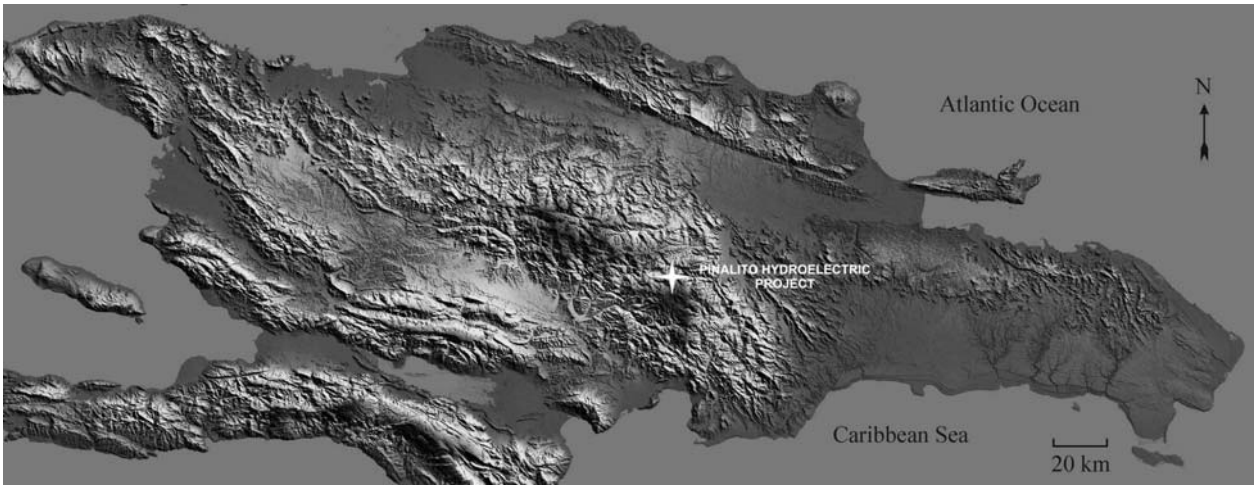

Figure 3 - Physiographic features of Hispaniola Island. Note markedly segmentation of landscape made of narrow and elongated mountain ranges and sedimentary basins limited by faults with WNW-ESE-trending. Source: Shuttle Radar Topography Mission (SRTM-90m).

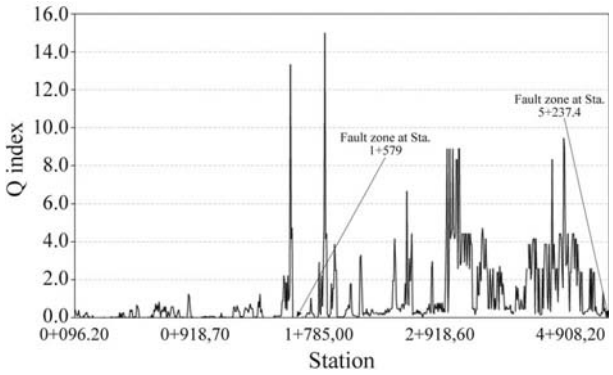

Figure 4 - Q index along Pinalito main hydroelectric tunnel, before the fault zone at Sta. 5+237.4.

5+237.40, and is mainly made of highly jointed andesitic tuff cut by minor clay and epidote-bearing faults.

6.2. Drainage

In order to relieve groundwater pressure, it was drilled fifty two drains at different locations comprising a half cone-like roof. The amount of it is concentrated in the hydraulic left sidewall of the tunnel alignment, a region where the incompetent zone seems to be wider according to geological drills (see Fig. 6). After a period of four months groundwater pressure decreased significantly, in contrast, groundwater influx was continuously growing until its highest value (~460 L/s) in the beginning of July (Fig. 7).

6.3. Spilling and grouting injections

Because of the extremely high groundwater influx into the tunnel and the rock collapse of the roof area over the TBM head two distinct resin grouting were injected. The polyurethane resin was firstly performed in order to water stopping while the urea-silicate resin was injected in order to fill unknown cavities, caused by the rapid groundwater leakage into the tunnel followed by a rock collapse. After controlling water and cavities, injections of cement and microcement (ultra-fine cement) slurries were performed in order to consolidate the fault zone. Pressures of injections varied from 0 to 200 bars.

Chemical resins were initially injected through thirty two spilling bars drilled approximately at four stations located in the back of the TBM, forming a half cone-like roof through the incompetent zone. The drill holes consumed 1.4 ton of both resins and its result couldn't still be evaluated.

Since the TBM went through the fault zone and was trapped by it, it was necessary to release and pull it back.

Table 1 - Relationship between TBM Push, Q index, rock class and rock support. Q index ranges derived exclusively from Pinalito Hydroelectric Project.

TBM Push (psi)	Q	Rock Class	Rock support
300	< 0.015	IV/V	Steel ribs
600	0.015-0.5	III	Systematic rock bolts and shotcrete
1.000	0.5-3	II	Rock bolts and shotcrete only localized
2.000	> 3	I	Unnecessary

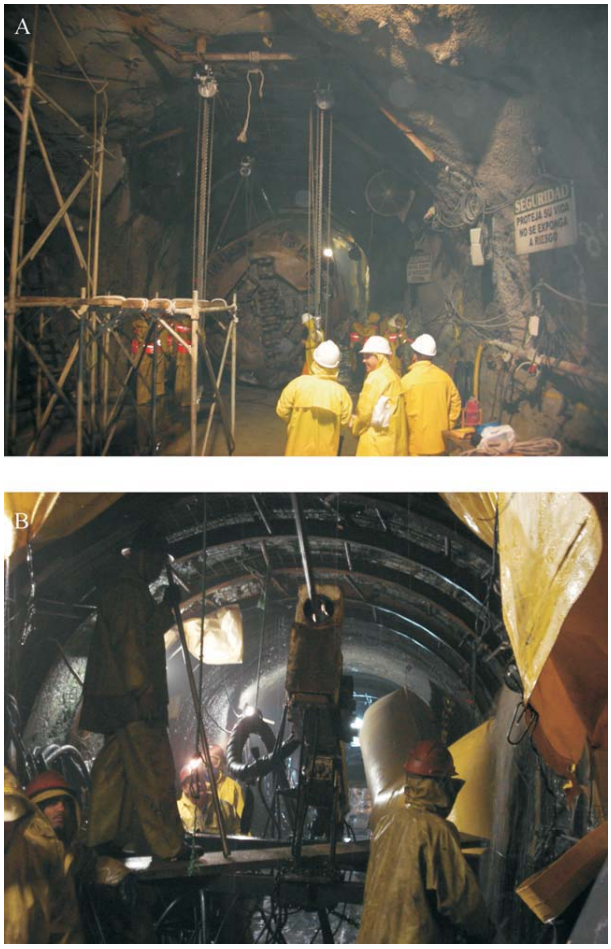

Figure 5 - A – TBM being disassembled (front view); B – External rock drilling adapted to operate during TBM entrapment.

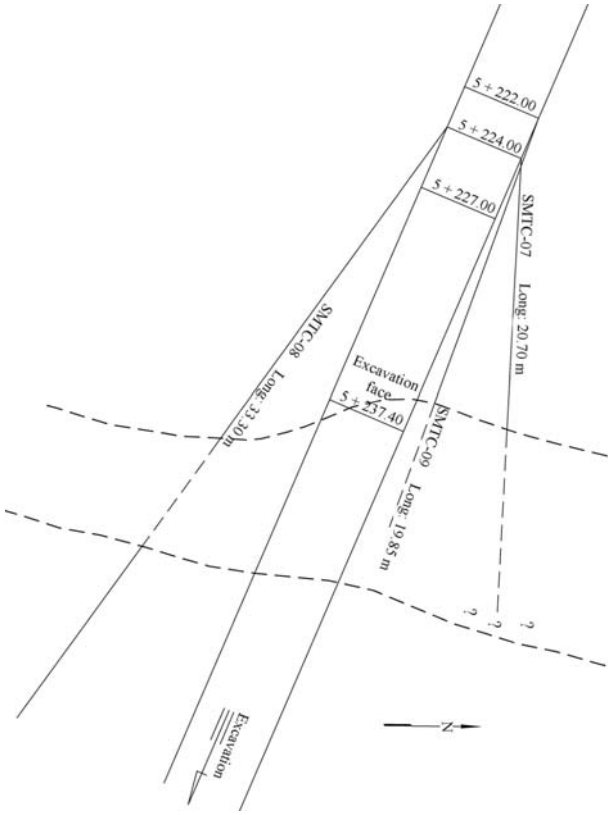

Figure 6 - Plain view of geological drills performed through the water fault zone (dash dot lines), Sta. 5+237.40 m. RQD = Rock Quality Designation.

Once the machine was free, it was observed a meaningful change of the groundwater flux in the excavation face, subsequently, was observed a sudden rock collapse that filled almost 70% of the released area ahead of the TBM (Fig. 8). In order to overcome it and carry on the excavation, collapsed material must be treated before consolidating the fault zone. The method found in order to stabilize the collapsed material was to set thirty one pipes of 1/2 and 2" of diameter straight into the collapsed material. All pipes were previously pierced with small holes in order to permit resin and cement slurries get into the collapsed material. Initially, it was made an attempt to injected 5.1 ton of cement/microcement slurries with different mixtures (water/cement) combined to additives; however, all of it ran away under the TBM, showing that groundwater was still present. Consequently, was performed the injection of 5.1 ton of polyurethane resin through the pipes until the absolute refuse of the rock mass by high pressure or inflow

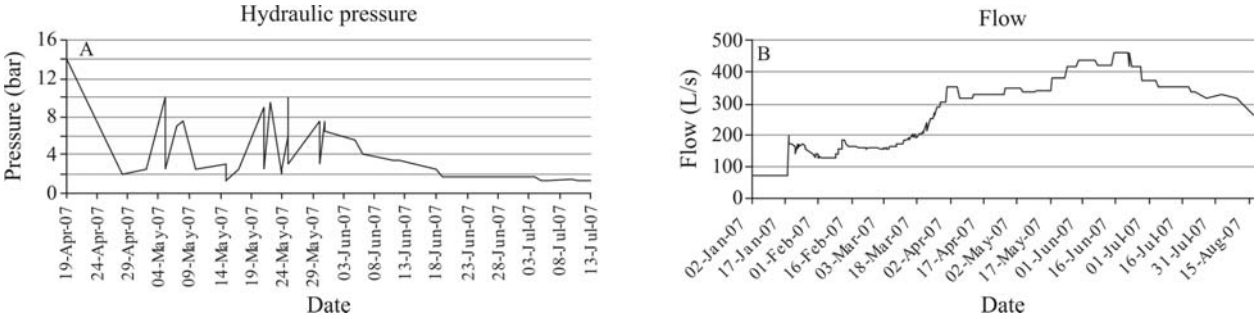

Figure 7 - Groundwater parameters: (A) hydraulic pressure (in bars); and (B) total groundwater flow (L/s). Parameters show opposite trend with time.

Figure 8 - Photo taken from the upper portion of the TBM head. It shows the ground condition ahead of the TBM after sudden rock collapse. Note fault content occupying almost 70% of the released area and a hanged spilling bar previously drilled through the fault zone.

Figure 9 - Wall of injection built at Sta. 5+237.40 m, in the Pinalito rock Tunnel. Note in the roof area, part of tubes/spilling bars previously drilled and remnants of polyurethane foam.

into the tunnel. Additionally, was drilled more twenty five spilling bars before consolidation of the fault zone get started. These consumed 3.4 ton of polyurethane resin and 1.6 ton of cement/microcement slurries.

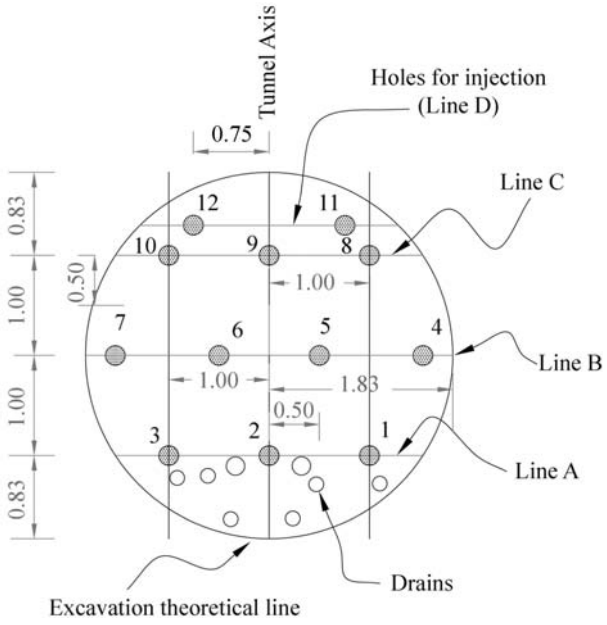

Figure 10 - Vertical section of the wall of injection at Sta. 5+237.40 m, Pinalito rock Tunnel. Note parallel lines of injection, from A to D, and drains placed in the base in order to release groundwater pressure.

Once the collapsed material was stabilized, the TBM was pulled back nearly three and a half meters and treatment of the fault zone could proceed. In order to increase efficiency of consolidation treatment, was opted to build two walls through the fault zone, not exactly the same, separated approximately of five meters, comprising 3.66 m of diameter and 1.0 m of wide, made of cement bags and shotcrete (Fig. 9). The walls comprise horizontal and parallel lines with holes of injection through the fault zone and drains in its base, in order to relieve groundwater pressure (Fig. 10). Because of the fault zone showed to be wider in the left sidewall of the tunnel alignment, special attention was given to holes placed in there. The injections started from the foot to the top of the wall and from the right to the left sidewall of the tunnel. It was consumed a total of 23.3 ton of cement/microcement and 1.1 ton of polyurethane.

7. Conclusions

The TBM re-started to work regularly in the middle of September of 2007. Ground treatment was successful and took six months to be concluded.

The sequence of procedures adopted to overcome the fault zone – (1) geological drilling; (2) drainage; and (3) spilling and grouting injections – showed to be very efficient, nevertheless slow and laborious.

The fault zone, with approximately eleven meters wide, consumed 11 ton of chemical resins and 30 ton of cement slurries. Pressure of resin injections varied from 20 to 200 bars while cement injections from 0 to 30 bars.

Geological, structural and hydrogeological investigations are indispensable procedures for rock tunnels projects, particularly adjoining plate tectonic boundaries, which combined with systematic probe drills and geophysics, can prevent many geological unfavorable situations, saving money and time.

Acknowledgments

The author would like to thank Sias Conradie, electrical chief of the TBM from South Africa, for helpful information about TBM specifications and excavation under difficult underground situations, and the geologist Jose Luis Torres from Ecuador, for geotechnical and hydrogeological tunnel data.

References

Barton, N.; Lien, R. & Lunde, J. (1974) Engineering classification of rock masses for the design of tunnel support. Rock Mechanics, v. 6(4), p. 186-236.

Bowin, C. (1966) Geology of central Dominican Republic: a case history of part of an island arc. Geological Society of America, v. 98, p. 11-84.

DeMets, C.; Jansma, P.; Mattioli, G.; Dixon, T.; Farina, F.; Bilham, R.; Calais, E. & Mann, P. (2000) GPS geodetic constraints on Caribean-North America plate motion. Geophysical Research Letters, v. 27, p. 437-440.

Dolan, J.F.; Mullins, H.T. & Wald, D.J. (1998) Active tectonics of the north-central Caribbean: Oblique collision, strain partitioning, and opposing subducted slabs. Dolan, J.F. & Mann, P. (eds) Active Strike Slip and Collisional Tectonics of the Northern Caribean Plate Boundary Zone. Geological Society of America Special Paper 326, p. 1-62.

Mann, P.; Draper, G. & Lewis, J.F. (1991) An Overview of the Geologic and Tectonic Development of Hispaniola. Geological Society of America, Special Paper 262, p. 1-27.

Mann, P.; Calais, E.; Ruegg, J.C.; DeMets, C.; Jansma, P.E. & Mattioli, G.S. (2002) Oblique collision in the northeastern Caribbean from GPS measurements and geological observations. Tectonics, v. 21(6), p. 1-26.

SOILS and ROCKS
An International Journal of Geotechnical and Geoenvironmental Engineering

Publication of
ABMS - Brazilian Association for Soil Mechanics and Geotechnical Engineering
ABGE - Brazilian Association for Engineering Geology and the Environment
SPG - Portuguese Geotechnical Society

Volume 32, N. 3, September-December 2009

Author index

Instructions to Authors

Category of the Papers

Soils and Rocks is the scientific journal edited by the Brazilian Society of Soil Mechanics and Geotechnical Engineering (ABMS) and by the Brazilian Society of Engineering and Environmental Geology (ABGE). The journal is intended to the divulgation of original research works from all geotechnical branches.

The accepted papers are classified either as an Article paper, a Technical Note, a Case Study, or a Discussion according to its content. An article paper is an extensive and conclusive dissertation about a geotechnical topic. A paper is considered as a technical note if it gives a short description of ongoing studies, comprising partial results and/or particular aspects of the investigation. A case study is a report of unusual problems found during the design, construction or the performance of geotechnical projects. A case study is also considered as the report of an unusual solution given to an ordinary problem. The discussions about published papers, case studies and technical notes are made in the Discussions Section.

When submitting a manuscript for review, the authors should indicate the category of the manuscript, and is also understood that they:

a) assume full responsibility for the contents and accuracy of the information in the paper;

b) assure that the paper has not been previously published, and is not being submitted to any other periodical for publication.

Manuscript Instructions

Manuscripts must be written in English. The text is to be typed in a word processor (MS Word or equivalent), using ISO A4 page size, left, right, top, and bottom margins of 25 mm, Times New Roman 12 font, and line spacing of 1.5. All lines and pages should be numbered. The text should be written in the third person.

The fist page of the manuscript is to include the title of the paper in English, followed by the names of the authors with the abbreviation of the most relevant academic title. The affiliation, address and e-mail is to be indicated below each author's name. An abstract of 200 words is to be written in English after the author's names. A list with up to six keywords at the end of the abstract is required.

Although alteration of the sequence and the title of each section may be required, it is suggested that the text contains the following sections: Introduction, Material and Methods, Results, Discussions, Conclusion, Acknowledgements, References and List of Symbols. A brief description of each section is given next.

Introduction: This section should indicate the state of the art of the problem under evaluation, a description of the problem and the methods undertaken. The objective of the work is to be clearly presented at the end of the section.

Materials and Methods: This section should include all information needed to the reproduction of the presented work by other researchers.

Results: In this section the data of the investigation should be presented in a clear and concise way. Figures and tables should not repeat the same information.

Discussion: The analyses of the results should be described in this section. **Conclusions**: The text of this section should be based on the presented data and in the discussions.

Acknowledgenments: If necessary, concise acknowledgements should be written in this section.

References: References to other published sources are to be made in the text by the last name(s) of the author(s), followed by the year of publication, similarly to one of the two possibilities below:

"*while Silva & Pereira (1987) observed that resistance depended on soil density*" or "*It was observed that resistance depended on soil density (Silva & Pereira, 1987).*"

In the case of three or more authors, the reduced format must be used, *e.g.*: Silva *et al.* (1982) or (Silva *et al.*, 1982). Two or more citations belonging to the same author(s) and published in the same year are to be distinguished with small letters, *e.g.*: (Silva, 1975a, b, c.). Standards must be cited in the text by the initials of the entity and the year of publication, *e.g.*: ABNT (1996), ASTM (2003).

Full references shall be listed alphabetically at the end of the text by the first author's last name. Several references belonging to the same author shall be cited chronologically. Some examples are listed next:

Papers: Bishop, A.W. & Blight, G.E. (1963) Some aspects of effective stress in saturated and unsaturated soils. Géotechnique, v. 13:2, p. 177-197.

Books: Lambe, T.W & Whitman, R.V. (1979) Soil Mechanics, SI Version, 2nd ed. John Wiley & Sons, New York, p. 553.

Book with editors: Sharma, H.D.; Dukes, M.T. & Olsen, D.M. (1990) Field measurements of dynamic moduli and Poisson's ratios of refuse and underlying soils at a landfill site. Landva A. & Knowles, G.D. (eds) Geotechnics of Waste Fills - Theory and Practice, American Society for Testing and Materials - STP 1070, Philadelphia, p. 57-70.

Proceedings (printed matter or CD-ROM): Jamiolkowski, M.; Ladd, C.C.; Germaine, J.T & Lancellotta, R. (1985) New developments in field and laboratory testing of soils. Proc. 11th Int. Conf. on Soil Mech. and Found. Engn., ISSMFE, San Francisco, v. 1, pp. 57-153.(specify if CD – ROM)

Thesis and dissertations: Lee, K.L. (1965) Triaxial Compressive Strength of Saturated Sands Under Seismic Loading Conditions. PhD Dissertation, Department of Civil Engineering, University of California, Berkeley, 521 p.

Standards: ASTM (2003) Standard Test Method for Particle Size Analysis of Soils - D 422-63. ASTM International, West Conshohocken, Pennsylvania, USA, 8 p.

Internet references: Soils and Rocks available at http://www.abms.com.br.

On line first publications must also bring the digital object identifier (DOI) at the end.

Figures shall be either computer generated or drawn with India ink on tracing paper. Computer generated figures must be accompanied by the corresponding digital file (.tif, .jpg, .pcx, etc.). All figures (graphs, line drawings, photographs, etc.) shall be numbered consecutively and have a caption consisting of the figure number and a brief title or description of the figure. This number should be used when referring to the figure in text. Photographs should be black and white, sharp, high contrasted and printed on glossy paper.

Tables shall be numbered consecutively in Arabic and have a caption consisting of the table number and a brief title. This number should be used when referring to the table in text. Units should be indicated in the first line of the table, below the title of each column. Abbreviations should be avoided. Column headings should not be abbreviated. When applicable, the units should come right below the corresponding column heading. Any necessary explanation can be placed as footnotes.

Equations shall appear isolated in a single line of the text. Numbers identifying equations must be flush with the right margin. International System (SI) units are to be used. The symbols used in the equations shall be listed in the List of Symbols. It is recommended that the used symbols

be in accordance with Lexicon in 8 Languages, ISSMFE (1981) and the ISRM List of Symbols.

The text of the submitted manuscript (including figures, tables and references) intended to be published as an article paper or a case history should not contain more than 30 pages formatted according to the instructions mentioned above. Technical notes and discussions should have no more than 15 and 8 pages, respectively. Longer manuscripts may be exceptionally accepted if the authors provide proper explanation for the need of the required extra space in the cover letter.

Discussion

Discussions must be written in English. The first page of a discussion paper should contain:

• The title of the paper under discussion in the language chosen for publication;

• Name of the author(s) of the discussion, followed by the position, affiliation, address and e-mail. The discusser(s) should refer himself (herself, themselves) as "the discusser(s)" and to the author(s) of the paper as "the author(s)".

Figures, tables and equations should be numbered following the same sequence of the original paper. All instructions previously mentioned for the preparation of article papers, case studies and technical notes also apply to the preparation of discussions.

Editorial Review

Each paper will be evaluated by reviewers selected by the editors according to the subject of the paper. The authors will be informed about the results of the review process. If the paper is accepted, the authors will be required to submit a version of the revised manuscript with the suggested modifications. If the manuscript is refused for publication, the authors will be informed about the reasons for rejection. In any situation comprising modification of the original text, classification of the manuscript in a category different from that proposed by the authors, or refusal for publication, the authors can reply presenting their reasons for disagreeing with the reviewers' comments

Submission

The author(s) must submit for review:

1. A hard copy of the manuscript to Editors - Soils and Rocks, Av. Prof. Almeida Prado, 532 – IPT, Prédio 54 – DEC/ABMS, 05508-901 - São Paulo, SP, Brazil. The first page of the manuscript should contain the identification of the author(s), or

2. The digital file of the manuscript, omitting the authors' name and any information that eventually could identify them, should be sent to **abms@ipt.br**. The following must be written in the subject of the e-mail message: "*Paper submitted to Soils and Rocks"*. The authors' names, academic degrees and affiliations should be mentioned in the e-mail message. The e-mail address from which the digital file of the paper was sent will be the only one used by the editors for communication with the corresponding author.

Follow Up

Authors of manuscripts can assess the status of the review process at the journal website (www.soilsandrocks.com.br) or by contacting the ABMS secretariat.

SOILS and ROCKS *An International Journal of Geotechnical and Geoenvironmental Engineering*

Volume 32, N. 3, September-December 2009

Table of Contents